






Goliath induces inflammation in obese mice by linking fatty acid β -oxidation to glycolysis

Shumeng Hao^{1,†} , Sulin Zhang^{2,†}, Jialin Ye^{1,†} , Lifan Chen², Yan Wang¹, Siyu Pei^{1,3}, Qingchen Zhu¹, Jing Xu¹, Yongzhen Tao¹, Neng Zhou⁴, Huiyong Yin¹ , Cai-Wen Duan⁴, Chaoming Mao⁵ , Mingyue Zheng^{2,*} & Yichuan Xiao^{1,**} 

Abstract

Obesity is associated with metabolic disorders and chronic inflammation. However, the obesity-associated metabolic contribution to inflammatory induction remains elusive. Here, we show that, compared with lean mice, CD4⁺ T cells from obese mice exhibit elevated basal levels of fatty acid β -oxidation (FAO), which promote T cell glycolysis and thus hyperactivation, leading to enhanced induction of inflammation. Mechanistically, the FAO rate-limiting enzyme carnitine palmitoyltransferase 1a (Cpt1a) stabilizes the mitochondrial E3 ubiquitin ligase Goliath, which mediates deubiquitination of calcineurin and thus enhances activation of NF-AT signaling, thereby promoting glycolysis and hyperactivation of CD4⁺ T cells in obesity. We also report the specific GOLIATH inhibitor DC-Gonib32, which blocks this FAO-glycolysis metabolic axis in CD4⁺ T cells of obese mice and reduces the induction of inflammation. Overall, these findings establish a role of a Goliath-bridged FAO-glycolysis axis in mediating CD4⁺ T cell hyperactivation and thus inflammation in obese mice.

Keywords FAO; glycolysis; Goliath; inflammation; obesity

Subject Categories Immunology; Metabolism; Post-translational Modifications & Proteolysis

DOI 10.15252/embr.202356932 | Received 2 February 2023 |

Accepted 8 February 2023 | Published online 2 March 2023

EMBO Reports (2023) 24: e56932

Introduction

Obesity is associated with a higher prevalence and a worse prognosis of several inflammatory diseases (Versini *et al*, 2014; Cox *et al*, 2015), including systemic lupus erythematosus (SLE), rheumatoid

arthritis, multiple sclerosis, and inflammatory bowel disease (Chaiamnuay *et al*, 2007; Kim *et al*, 2017; Singh *et al*, 2017; Van Raemdonck *et al*, 2018). During the progression of obesity, the adipose tissue secretes an increased number of adipokines, which are responsible for a proinflammatory state for innate immune activation as well as deregulation of CD4⁺ T help (Th) cell differentiation, resulting in accumulated proinflammatory Th1 and Th17 cells, whereas reduced anti-inflammatory Th2 and Treg cells in adipose tissue (Kaminski & Randall, 2010; Sell *et al*, 2012; McLaughlin *et al*, 2017; Reilly & Saltiel, 2017). Despite these progresses, published studies have mainly focused on the inflammation in adipose tissues in the context of obesity, while the impact of obesity on proinflammatory induction in other peripheral tissues is not clear.

CD4⁺ T cells are the primary effector cells for the induction of inflammation *in vivo*. The efficient activation and effector function of CD4⁺ T cells largely rely on the aerobic glycolysis induced by their utilization of glucose (Frauwirth *et al*, 2002; Wang *et al*, 2011; Gerriets & Rathmell, 2012; Chang *et al*, 2013; Macintyre *et al*, 2014). Targeting glycolysis has been shown to be a promising strategy to prevent CD4⁺ T cell-mediated inflammatory responses, such as administration of glycolysis inhibitor 2-deoxy-D-glucose (2-DG) reversed the proinflammatory manifestations in many related mouse models (Shi *et al*, 2011; Yin *et al*, 2015). Unlike glucose, the utilization of fatty acids occurs mainly in CD8⁺ T cells (Lochner *et al*, 2015), in which FAO is essential for the development of memory cells (Pearce *et al*, 2009). Blocking FAO selectively impaired the survival of CD8⁺ memory T cells, but not effector cells (van der Windt *et al*, 2012). A recent study suggested that diet-induced obesity promoted the activation and memory differentiation of CD4⁺ T cells (Endo *et al*, 2015; Mauro *et al*, 2017), and inhibition of FAO with etomoxir prevented the activation of CD4⁺ T cells in mice that fed with saturated fatty acid-enriched diet (Mauro *et al*, 2017), suggesting FAO may also affect CD4⁺ T cell effector function during

1 CAS Key Laboratory of Tissue Microenvironment and Tumor, Shanghai Institute of Nutrition and Health, University of Chinese Academy of Sciences, Chinese Academy of Sciences, Shanghai, China

2 Drug Discovery and Design Center, State Key Laboratory of Drug Research, Shanghai Institute of Materia Medica, University of Chinese Academy of Sciences, Chinese Academy of Sciences, Shanghai, China

3 Department of Thoracic Surgical Oncology, Shanghai Lung Cancer Center, Shanghai Chest Hospital, Shanghai Jiao Tong University School of Medicine, Shanghai, China

4 Key Laboratory of Pediatric Hematology and Oncology Ministry of Health and Pediatric Translational Medicine Institute, Shanghai Children's Medical Center, Shanghai Jiao Tong University School of Medicine, Shanghai, China

5 Department of Nuclear Medicine, The Affiliated Hospital of Jiangsu University, Zhenjiang, China

*Corresponding author. Tel: +86 21 50806600; E-mail: myzheng@simm.ac.cn

**Corresponding author. Tel: +86 21 54923276; E-mail: ycxiao@sibs.ac.cn

†These authors contributed equally to this work

obesity. Obesity also involves an accumulation in the mass of white adipose tissue, leading to increased levels of fatty acids, cholesterol, and other lipid metabolites (Rosen & Spiegelman, 2014; Mishra et al, 2016; Vishvanath & Gupta, 2019). However, whether and how these lipid metabolites can be utilized to fuel CD4⁺ T cell activation/proliferation for their effector function that drives inflammation still remain elusive. Considering the essential role of glycolysis on CD4⁺ T cell effector function, it is likely that FAO has some unknown association with glycolysis to boost the functional activation of CD4⁺ T cells during obesity. However, the connection between FAO and glycolysis and the signals driving this process in CD4⁺ T cells in potentiating obesity-related inflammation are poorly understood.

In this study, we established an FAO-glycolysis axis that was bridged through the mitochondrial E3 ubiquitin ligase Goliath, in promoting CD4⁺ T cell activation/proliferation under obese condition, thereby potentiating their induction of inflammation.

Results

Obesity induces a proinflammatory feature of CD4⁺ T cells through glycolysis

To explore the contribution of obesity to CD4⁺ T cell activation and proliferation, we generated the obese mice feeding with high-fat diet (HFD) or naturally aged obese mice feeding with normal diet. The results showed that obesity greatly promoted T cell receptor (TCR)-induced activation and proliferation of naïve CD4⁺ T cells but not in CD8⁺ T cells isolated from spleen and lymph nodes, as manifested by increased percentage of proliferating cells and enhanced *Il2/Ifn γ* expression upon TCR stimulation in CD4⁺ T cells derived from either diet-induced obese mice or naturally aged obese mice (Fig 1A–D, and Appendix Fig S1A and B). The efficient activation of CD4⁺ T cells largely relies on the aerobic glycolysis (Frauwrith et al, 2002; Gerriets & Rathmell, 2012). Interestingly, we found that CD4⁺ T cells from HFD-induced or aged obese mice or obese human with TCR stimulation exhibited enhanced levels of glycolysis, as measured by the extracellular acidification rate (ECAR), glycolytic flux, and glycolysis-related gene expression (Fig 1E–G and Appendix Fig S1C–E). However, the oxidative phosphorylation (OXPHOS) measured by oxygen consumption rate (OCR), labeled TCA cycle intermediates, the activity of lactate dehydrogenase (LDH) and pyruvate dehydrogenase (PDH) measured by gas chromatography–mass spectrometry (GC/MS) were comparable in CD4⁺ T cells from lean and obese mice, which suggested that obesity specially enhanced aerobic glycolysis, but not TCA cycle, in CD4⁺ T cells (Appendix Fig S1F–I). In addition, obesity increased the protein levels of glycolysis intermediate enzyme HK2 in CD4⁺ T cells upon TCR stimulation (Appendix Fig S1J), which further implied obesity promoted the activity of intermediate enzymes and thus the glycolytic flux. Moreover, after treatment with glycolysis inhibitor 2-DG or D-galactose (D-gal), TCR-induced proliferation and activation of CD4⁺ T cells from obese mice were significantly inhibited, with no obvious difference when compared to naïve CD4⁺ T cells from lean mice (Fig 1H and I, and Appendix Fig S1K and L). These data implied that obesity specifically drives TCR-induced CD4⁺ T cell activation/proliferation through enhanced glycolysis.

To examine whether CD4⁺ T cells from obese mice have enhanced ability to induce inflammation, we adoptively transferred the same amount of lean or obese mice (C57BL/6 background)-derived CD45.2⁺CD4⁺ T cells into BM12/SJL mice (CD45.1⁺CD45.2⁺) to induce an inflammation model, which will exclude the influence of *in vivo* complex microenvironment of obesity mice. Since the BM12 mice differ from C57BL/6 mice by three amino acid substitutions in the β -chain of the MHC class II molecule I-A, this adoptive transfer will induce the expansion of donor-derived T follicular helper (Tfh) and recipient-derived germinal center (GC) B cells and plasma cells, resulting in the production of antinuclear antibody and IgG deposits in the kidneys of recipient mice, thereby leading to the induction of chronic GVHD with symptoms closely resembling lupus-like disease (Wang et al, 2016; Liu et al, 2018; Huang et al, 2021). As expected, the percentages of lean- and obese-derived CD4⁺ T cells into regulatory T (Treg), Th1, Th17, and Th2 cells in the recipient mice were comparable, while the frequencies and absolute numbers of the transferred CD45.2⁺ Tfh cells, recipient GC B and plasma cells were greatly increased in obese CD4⁺ T cells group. Accordingly, BM12 recipient mice immunized with CD4⁺ T cells from obese mice markedly increased the production of serum antibodies and showed more IgG deposition in the kidney as compared to the recipient mice immunized with lean CD4⁺ T cells. In addition, 2-DG-induced glycolysis inhibition greatly suppressed obesity-induced inflammation with compromised *in vivo* Tfh differentiation, GC reactions, and abolished these differences between lean and obese conditions (Fig 1J–L and Appendix Fig S1M). These results collectively suggested that enhanced glycolysis is responsible for the promoted proinflammatory feature of CD4⁺ T cells from obese mice.

Obesity-elevated basal FAO promotes CD4⁺ T cell glycolysis

To figure out how obesity drives glycolysis in CD4⁺ T cells, we performed RNA-sequencing to analyze the transcriptome of lean and obese-derived splenic CD4⁺ T cells. Gene ontology (GO) analysis revealed that genes involved in inflammatory responses and lipid metabolism, especially that related to fatty acid metabolism, were enriched in CD4⁺ T cells from obese mice as compared to lean mice (Appendix Fig S2A). We also observed that there was more lipid accumulation as measured by BODIPY staining in CD4⁺ T cells from obese mice when compared to lean mice (Fig 2A and B). The heatmap showed that CD4⁺ T cells from obese mice had enhanced expression of genes related to fatty acid uptake, synthesis, and β -oxidation (Fig 2C). Consistently, naïve CD4⁺ T cells from obese mice exhibited markedly increased basal FAO level compared with naïve CD4⁺ T cells from lean mice (Fig 2D and E). Accordingly, quantitative real-time PCR (qRT-PCR) showed the increased expression of FAO-related genes in CD4⁺ T cells from obese mice and obese human (Fig 2F, and Appendix Fig S2B and C), which further confirmed the elevated basal FAO in CD4⁺ T cells from obese mice. In addition, treatment with short-chain fatty acids did not affect the protein levels of FAO rate-limiting enzyme carnitine palmitoyltransferase 1a (Cpt1a) and failed to further increase the FAO levels in CD4⁺ T cells either under LN or OB condition and the FAO difference was only observed in CD4⁺ T cells between LN condition and OB condition, which excluded the possibility of short-chain fatty acids in promoting endogenous FAO under obese condition (Appendix Fig S2D–F).

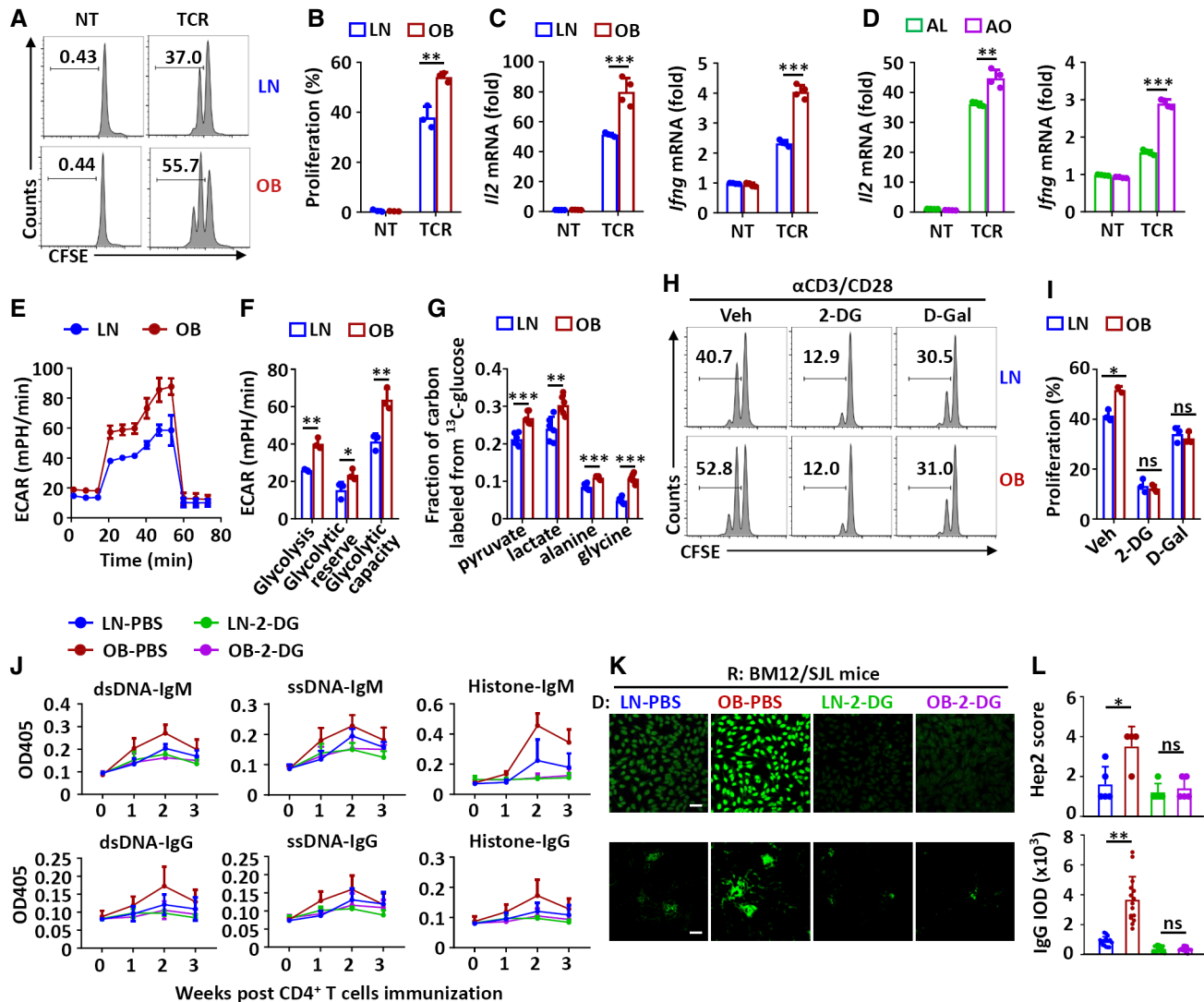


Figure 1. Obesity potentiates CD4⁺ T cell-mediated inflammation through enhanced glycolysis.

A, B Proliferation analysis of naïve CD4⁺ T cells isolated from spleen and lymph nodes of normal-diet-fed lean (LN) and high-fat-diet-fed obese (OB) mice that were left nontreated (NT) or stimulated with α -CD3/28 (TCR, 1/1 μ g/ml) for 3 days ($n = 3$ or 4, biological replicates). Data are presented as the representative FACS histograms (A) and statistical graph (B).

C, D qRT-PCR analysis of *Ii2* and *Iifng* mRNA in CD4⁺ T cells from LN and OB mice (C) or from aged lean (AL, 17-month-old) and aged obese (AO, 17-month-old) mice (D), then stimulated with TCR (1/1 μ g/ml) for 6 h. For AL and AO mice, mice were fed with a normal diet for 17 months, then divided into AL (≤ 35 g) and AO (≥ 45 g) mice based on body weight ($n = 3$ or 4, biological replicates).

E, F Extracellular acidification rates (ECAR) measurements of naïve CD4⁺ T cells from LN and OB mice upon TCR (1/1 μ g/ml) stimulation for 24 h ($n = 3$ or 4, biological replicates). The statistical results are presented as a bar graph (F).

G Fractions of labeled metabolites in glycolysis from the [¹³C₆]glucose in CD4⁺ T cells from lean and obese mice upon TCR (1/1 μ g/ml) stimulation for 24 h ($n = 3$ or 4, biological replicates).

H, I Proliferation analysis of CD4⁺ T cells from lean and obese mice with the indicated treatment upon TCR (1/1 μ g/ml) stimulation for 3 days ($n = 3$ or 4, biological replicates). Veh, vehicle; 2-DG, 5 mM; D-gal, 20 mM.

J–L BM12/SJL mice (recipient, R) were immunized with CD4⁺ T cells from LN and OB mice (donor, D) and then intraperitoneally injected once every day with 2-DG (200 mg/kg) or PBS for 3 weeks. Enzyme-linked immunosorbent assay (ELISA) of anti-dsDNA, anti-ssDNA, and antihistone IgG or IgM in serum from the immunized mice at the indicated time (J). Immunofluorescent analysis of antinuclear antibody (ANA) in serum (top) and IgG deposition in the kidney (bottom) ($n = 4$ or 5, biological replicates). Scale bar: 50 μ m. Data are presented as immunofluorescent images (K) and quantification of bar graphs (L).

Data information: All data are representative of at least three individual experiments. Statistics, two-tailed Student's t-test; ns, not significant, * $P < 0.05$, ** $P < 0.01$, *** $P < 0.001$. Error bars represent SD.

Next, we examined whether increased basal FAO could promote CD4⁺ T cell glycolysis upon stimulation. Published study has demonstrated that fenofibrate (FF) is a PPAR α agonist, which enhanced

FAO in CD8⁺ T cells (Zhang *et al.*, 2017). Interestingly, treatment with fenofibrate also promoted TCR-induced glycolytic metabolism and TCA cycle without affecting the activity of LDH and PDH, and

TCR-induced cellular proliferation and activation of naïve CD4⁺ T cells were also enhanced accordingly (Fig 2G–K and Appendix Fig S2G–J). By contrast, treatment with etomoxir, a selective inhibitor of Cpt1a, dramatically suppressed obesity-enhanced glycolysis and proliferation without inhibiting TCA cycle and the activities of LDH and PDH and abolished the difference between lean and obese mice (Fig 2L–P and Appendix Fig S2K–M). Considering the effect of FF or

etomoxir on CD4⁺ T cell effector function, these data further confirmed that obesity-promoted CD4⁺ T cell effector function is attributed from promoted aerobic glycolysis but not rely on downstream TCA cycle production or LDH/PDH activities. Moreover, obesity failed to promote TCR-induced glycolysis and cellular proliferation in *Cpt1a* deficiency CD4⁺ T cells (Fig 2Q and R, and Appendix Fig S3A), which excluded the off-target effect of etomoxir (Raud et al,

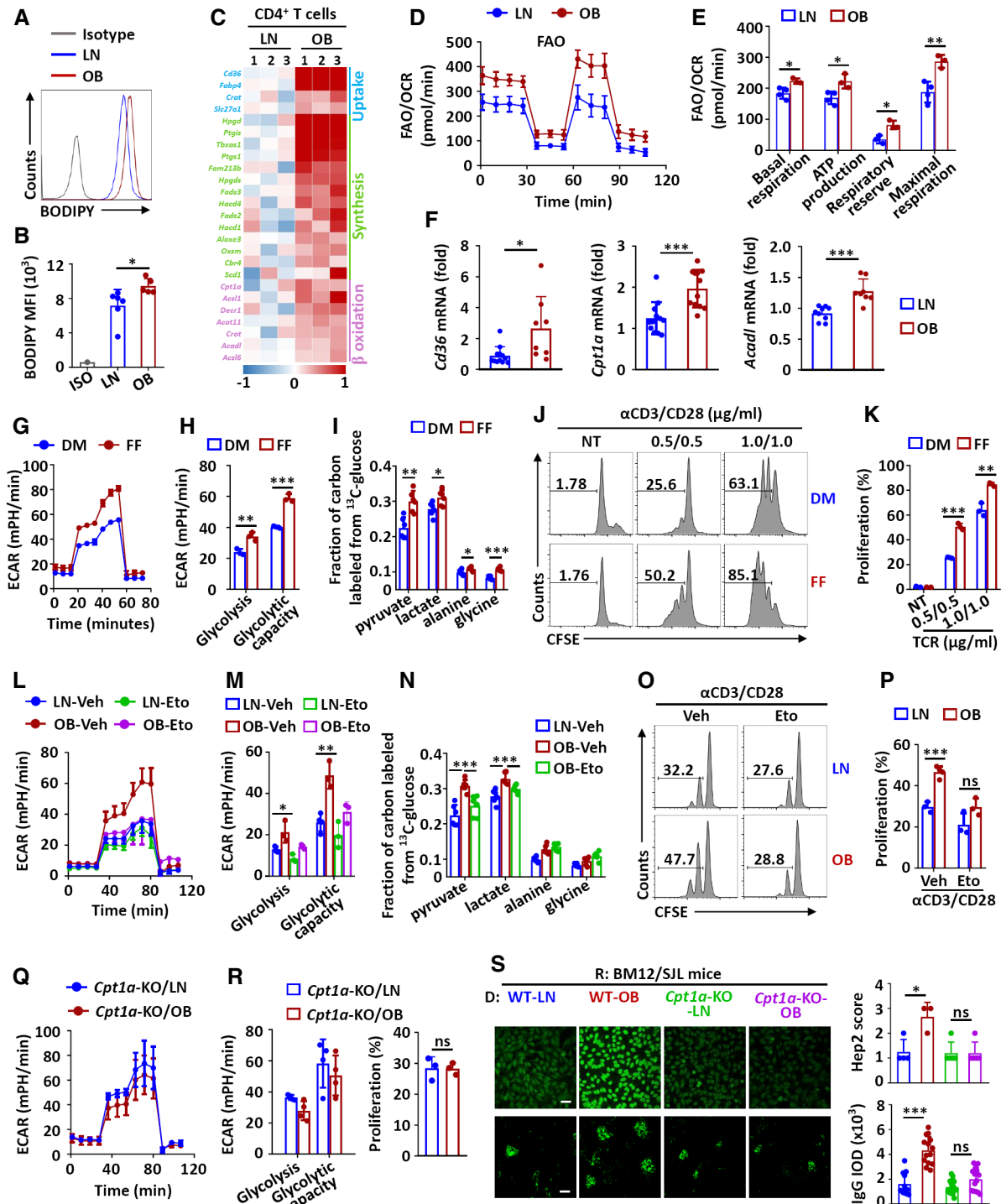


Figure 2.

Figure 2. Obesity-elevated basal FAO promotes CD4⁺ T cell glycolysis.

- A, B FACS of lipid droplets using BODIPY staining in CD4⁺ T cells *ex vivo* from lean (LN, *n* = 6, biological replicates) and obese (OB, *n* = 5, biological replicates) mice.
- C Heatmap showing the differentially expression genes (DEGs) involved in fatty acid metabolism in splenic naïve CD4⁺ T cells from lean and obese mice (*n* = 3, biological replicates).
- D, E Measurements of basal FAO by oxygen consumption rates (OCR) assay in naïve CD4⁺ T cells *ex vivo* from LN and OB mice (*n* = 3, biological replicates). The statistical results are presented as a bar graph (E).
- F qRT-PCR analysis of the transcriptional levels of indicated genes in fatty acid metabolism in CD4⁺ T cells *ex vivo* from LN and OB mice (*n* = 3 or 4, biological replicates).
- G, H ECAR measurements of glycolysis of naïve CD4⁺ T cell that treated with DMSO or fenofibrate (FF, 5 μ M) that stimulated with α -CD3/CD28 (TCR, 1/1 μ g/ml) for 24 h (*n* = 3, biological replicates). The statistical results are presented as a bar graph (H).
- I Fractions of labeled metabolites in glycolysis from the [U-¹³C₆]glucose in CD4⁺ T cells treated with DMSO or fenofibrate (FF, 5 μ M) that stimulated with α -CD3/CD28 (TCR, 1/1 μ g/ml) for 24 h (*n* = 3 or 4, biological replicates).
- J, K Cellular proliferation analysis of naïve CD4⁺ T cell that treated with DMSO or fenofibrate (FF, 5 μ M), and stimulated with different α -CD3/CD28 (0, 0.5/0.5, 1.0/1.0 μ g/ml) for 3 days (*n* = 3, biological replicates). The statistical results are presented as a bar graph (K).
- L, M ECAR measurements of glycolysis of naïve CD4⁺ T cell from LN and OB mice treated with vehicle or etomoxir (Eto, 150 μ M) that stimulated with α -CD3/CD28 (TCR, 1/1 μ g/ml) for 24 h (*n* = 3, biological replicates). The statistical results are presented as a bar graph (M).
- N Fractions of labeled metabolites in glycolysis from the [U-¹³C₆]glucose in CD4⁺ T cells from LN and OB mice treated with vehicle or etomoxir (Eto, 150 μ M) that stimulated with α -CD3/CD28 (TCR, 1/1 μ g/ml) for 24 h (*n* = 3, biological replicates).
- O, P Cellular proliferation analysis of naïve CD4⁺ T cell from LN and OB mice that treated with DMSO or fenofibrate (FF, 5 μ M) stimulated with α -CD3/CD28 concentration (TCR, 1/1 μ g/ml) for 3 days (*n* = 3, biological replicates). The statistical results are presented as a bar graph (P).
- Q, R ECAR measurements of glycolysis and cellular proliferation analysis of *Cpt1a*-KO naïve CD4⁺ T cells from lean and obese mice that stimulated with α -CD3/CD28 (TCR, 1/1 μ g/ml) for 24 h (ECAR) or 3 days (proliferation) (*n* = 3, biological replicates). The statistical results are presented as a bar graph (R).
- S BM12/SJL mice (recipient, R) were adoptively transferred with CD4⁺ T cells from WT and *Cpt1a*-KO lean or obese mice (donors, D) to induce inflammation. The anti-nuclear antibody (ANA) in serum (top, scale bar: 50 μ m) and the kidney IgG deposition (bottom, scale bar: 50 μ m) were visualized using immunofluorescence (*n* = 4 or 5, biological replicates). Data are presented as Immunofluorescent images (left) and quantification bar graphs (right).

Data information: All data are representative of at least three individual experiments. Statistics, two-tailed Student's *t*-test; ns, not significant, **P* < 0.5, ***P* < 0.01, ****P* < 0.001. Error bars represent SD.

2018). Accordingly, *Cpt1a* deficiency in CD4⁺ T cells compromised the obesity-induced exaggeration of inflammation (Fig 2S). Similarly in normal-diet feeding lean mice, CD4⁺ T cells that isolated from adipose tissues showed elevated basal FAO levels along with enhanced gene expression related to T cell activation and glycolysis upon TCR stimulation as compared to CD4⁺ T cells from spleen (Appendix Fig S3B–D). Together, these results suggested that the *in vivo* high-fat environment shapes the feature of elevated cellular basal FAO, which in turn promoted the glycolysis level for cellular activation/proliferation upon TCR stimulation in CD4⁺ T cell during obesity.

FAO promotes Goliath-induced CaN deubiquitination

To dissect the molecular mechanism by which FAO promoting TCR-induced CD4⁺ T cell glycolysis during obesity, we examined the signaling activation in naïve CD4⁺ T cells upon TCR stimulation. The results showed that obesity affected neither TCR-induced upstream signaling activation like Zap70, Lat, and PLC γ , nor downstream NF- κ B, PI3K-AKT, MAPK, mTOR, and calcium flux activation (Appendix Fig S4A and B). However, NF-AT activation was specifically enhanced, as reflected by increased nuclear translocation of NFATc1/2, in naïve CD4⁺ T cells from obese mice that stimulated with TCR or PMA/Ionomycin (P/I) as compared to lean mice (Fig 3A and Appendix Fig S4C). Conversely, treatment with FAO inhibitor etomoxir inhibited TCR-induced NF-AT activation in naïve CD4⁺ T cells (Fig 3B). Moreover, PPAR α agonist fenofibrate treatment promoted P/I-induced NF-AT activation in WT naïve CD4⁺ T cells, but failed to do the same in *Cpt1a*-deficient cells (Fig 3C). Calcineurin (CaN) is a calcium-activated protein phosphatase that plays a central role in modulating downstream NF-AT activation, and TCR- or P/I-induced CaN deubiquitination is critical to induce NFATc1/2 nuclear translocation and then glycolytic metabolism in T cells

(Macian, 2005; Vaeth *et al*, 2017; Zhang *et al*, 2019). Interestingly, we found that CaN deubiquitination was dramatically inhibited in etomoxir-treated naïve CD4⁺ T cells, whereas fenofibrate promoted this effect, as compared to control naïve CD4⁺ T cells (Fig 3D and E). Accordingly, treatment with CaN inhibitor cyclosporin (CsA) or FK506 sharply suppressed obesity-promoted NF-AT activation and glycolysis and abolished the difference between lean and obese naïve CD4⁺ T cells (Fig 3F–H and Appendix Fig S4D). Collectively, these data suggested that FAO promoted NF-AT activation and then glycolysis through inducing CaN deubiquitination in CD4⁺ T cells.

Since FAO occurs in mitochondria (Lochner *et al*, 2015; Xiong, 2018), we speculated that E3 ligases or deubiquitinases (DUBs) located in mitochondria may regulate CaN deubiquitination and thus NF-AT activation. We therefore performed a luciferase assay to examine P/I-induced NF-AT transcriptional activity after knocking down all the reported mitochondrial E3 ligases/DUBs, respectively, in HEK293T cells. The results revealed that USP30 knockdown significantly promoted, whereas knockdown of the E3 ligase GOLIATH inhibited, P/I-induced NF-AT luciferase activity (Fig 3I). Although USP30 can bind to CaN, its overexpression failed to induce CaN deubiquitination in 293 T cells (Appendix Fig S4E and F). Interestingly, GOLIATH specifically bind to CaN but not to calmodulin, and its overexpression greatly promoted CaN deubiquitination dependent on its E3 ligase activity (Appendix Fig S4G–I); we thus focus the following study on GOLIATH. In mouse primary CD4⁺ T cells, immunofluorescence confirmed the localization of Goliath protein was in mitochondria (Fig 3J). Due to no available immunoblot antibody to detect endogenous Goliath protein in T cells, we generated *GOLIATH*-knockdown Jurkat T cells that transfected with HA-tagged *GOLIATH*, in which we also confirmed the CaN-GOLIATH association through coimmunoprecipitation (Co-IP) analysis (Fig 3K). To

confirm the function of Goliath in mediating endogenous CaN deubiquitination, we generated conditional knockout (KO) mice to specially delete Goliath in T cells (Appendix Fig S5A and B). As expected, *Goliath* deficiency greatly suppressed CaN deubiquitination triggered by TCR or P/I stimulation (Fig 3L and Appendix Fig S5C).

Therefore, these data identified a mitochondrial E3 ligase Goliath in mediating CaN deubiquitination in CD4⁺ T cells.

Because Goliath is an E3 ubiquitin ligase, we speculated the existence of a DUB that is activated by Goliath for inducing CaN deubiquitination. To identify this DUB, we performed unbiased mass

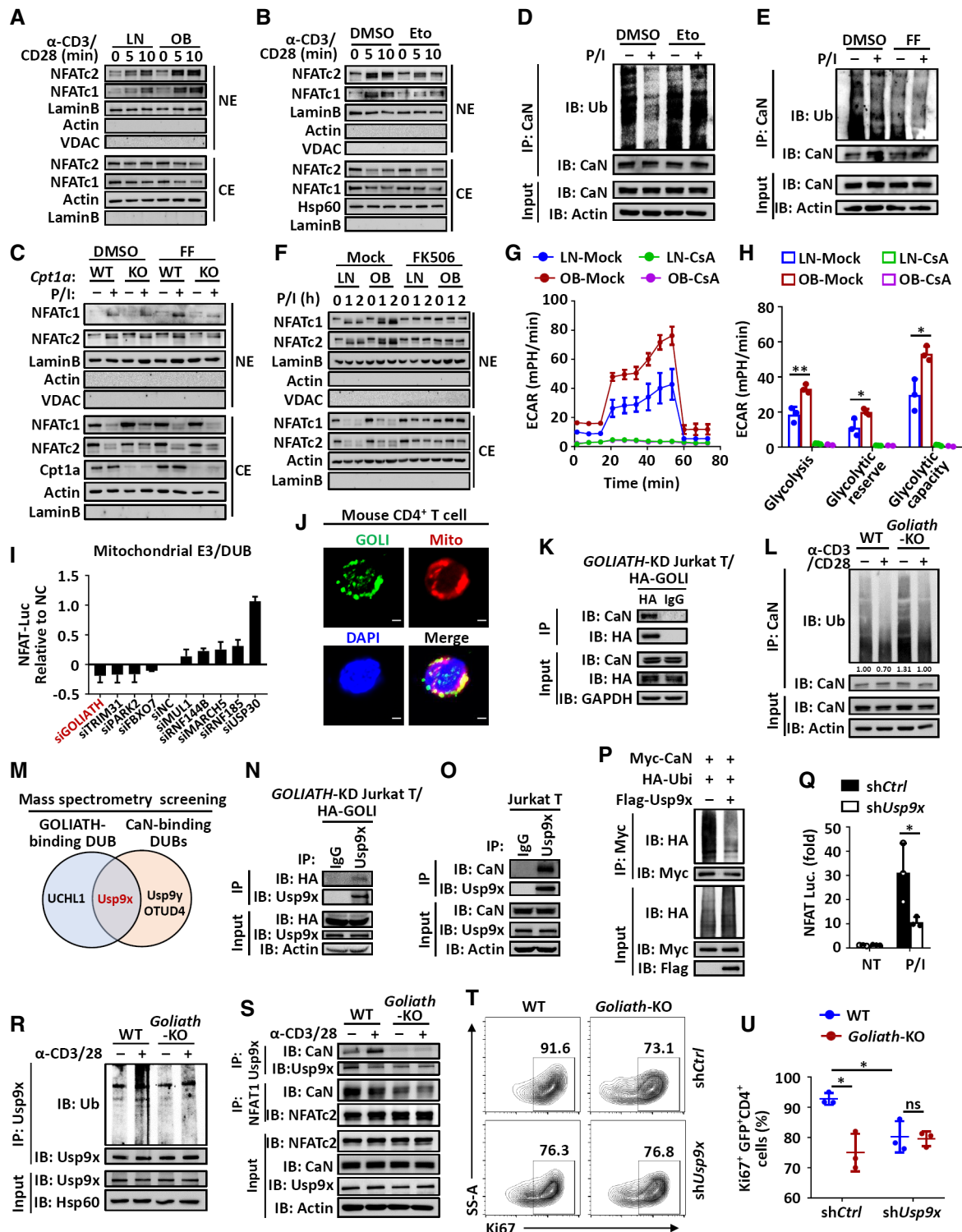


Figure 3.

Figure 3. FAO promotes Goliath-induced CaN deubiquitination and NF-AT activation.

- A–C Immunoblot analysis of cytoplasmic and nuclear NF-AT levels in naïve CD4⁺ T cells from lean (LN) and obese (OB) mice (A), or in naïve CD4⁺ T cells with DMSO or etomoxir (Eto, 150 μ M) pretreatment for 6 h (B), or in WT and *Cpt1a*-KO naïve CD4⁺ T cells with DMSO or fenofibrate (FF, 5 μ M) pretreatment for 6 h (C), which activated by α -CD3/28 (5/5 μ g/ml) or PMA/Ionomycin (P/I, 10/100 ng/ml) for the indicated time points.
- D, E Endogenous ubiquitination of CaN in naïve CD4⁺ T cells treated with DMSO and Eto (150 μ M) (D) or fenofibrate (FF, 5 μ M) (E), then stimulated with (+) or without P/I (10/100 ng/ml) (–).
- F Immunoblot analysis of cytoplasmic and nuclear NF-AT levels in naïve CD4⁺ T cells from LN and OB mice with Mock or FK506 (100 nM) treatment, then stimulated with (+) or without P/I (10/100 ng/ml) (–).
- G, H ECAR measurements of glycolysis in naïve CD4⁺ T cells from LN and OB mice treated with mock or CsA (5 μ M) under α -CD3/28 (1/1 μ g/ml) stimulation for 24 h ($n = 3$, biological replicates). The statistical results are presented as a bar graph (H).
- I NF-AT luciferase activity in HEK293T cells transfected with luciferase reporter and siRNAs targeting the indicated mitochondrial E3 ligases/deubiquitinases (DUBs), then stimulated by P/I (10/100 ng/ml) for 3 h ($n = 3$, biological replicates).
- J Confocal microscopic analysis of Goliath localization in murine CD4⁺ T cells. Scale bar: 2 μ m. GOLI, Goliath; Mito, mitochondria tracker.
- K Coimmunoprecipitation (Co-IP) analysis of the interaction between Goliath and CaN in GOLIATH-knockdown Jurkat T cells that reconstituted with HA-tagged GOLIATH.
- L Endogenous ubiquitination of CaN in WT and *Goliath*-deficient CD4⁺ T cells that were left unstimulated (–) or stimulated (+) with α -CD3/28 (5/5 μ g/ml).
- M Mass spectrometry screening of Goliath- and CaN-binding DUBs in HEK293T cells transfected with HA-GOLIATH and Flag-CaN.
- N, O Co-IP analysis of interactions between Usp9x and GOLIATH or CaN in GOLIATH-knockdown Jurkat T cells reconstituted with HA-tagged GOLIATH or in Jurkat T cells.
- P Ubiquitination of Usp9x in HEK293T cells transfected with indicated expression plasmids.
- Q NF-AT luciferase activity in control and *Usp9x*-knockdown HEK293T cells that left nontreated (NT) or stimulated by P/I (10/100 ng/ml) for 3 h.
- R Endogenous ubiquitination of Usp9x in WT and *Goliath*-deficient CD4⁺ T cells that were left unstimulated (–) or stimulated (+) with α -CD3/28 (5/5 μ g/ml).
- S Co-IP analysis of the interactions between CaN and Usp9x or NFATc2 and CaN in WT and *Goliath*-KO CD4⁺ T cells that were left unstimulated (–) or stimulated (+) with α -CD3/28 (5/5 μ g/ml).
- T, U Proliferation analysis of WT and *Goliath*-deficient CD4⁺ T cells infected with control (shCtrl) or *Usp9x*-specific shRNA upon α -CD3/28 (1/1 μ g/ml) stimulation for 3 days ($n = 3$, biological replicates).

Data information: All data are representative of at least three individual experiments. Statistics, two-tailed Student's *t*-test; * $P < 0.5$, ** $P < 0.01$. Error bars represent SD. Source data are available online for this figure.

spectrometry (MS) screening to look for the DUB that binds to both GOLIATH and CaN, and USP9x was the only DUB fitting the criteria (Fig 3M), which was confirmed that Usp9x not only bound to GOLIATH but also interacted with CaN in Jurkat T cells (Fig 3N and O). In addition, we identified that Usp9x specifically removed K6- and K63-linked polyubiquitination of CaN (Fig 3P and Appendix Fig S5D), and knockdown of Usp9x significantly reduced NF-AT transcriptional activity (Fig 3Q). Moreover, PPAR α agonist fenofibrate treatment markedly promoted, whereas *Goliath* deficiency abolished endogenous K63-linked ubiquitination of Usp9x in CD4⁺ T cells upon P/I or TCR stimulation (Fig 3R, and Appendix Fig S5E and F). Accordingly, the associations of CaN with Usp9x or NFATc2 were markedly suppressed in *Goliath*-deficient CD4⁺ T cells as compared to WT cells (Fig 3S). Consequently, Usp9x knockdown not only suppressed CD4⁺ T cell proliferation but also abolished the difference between WT and *Goliath*-deficient CD4⁺ T cells upon TCR stimulation (Fig 3T and U). These data collectively identified the E3 ligase Goliath as a mediator in activating Usp9x to induce CaN deubiquitination, thereby promoting NF-AT activation and cellular proliferation in CD4⁺ T cells.

Goliath potentiates obesity-induced T cell glycolysis and inflammation

We next applied WT and *Goliath* conditional KO mice to study the Goliath function in CD4⁺ T cells in the context of obesity. *Goliath* deficiency affected neither T cell development, maturation, and memory T cell generation in spleen or lymph nodes under normal diet condition, nor the calcium flux, CaN phosphorylation, the activation of Zap70, Lat, AKT, MAP kinases, and GSK3 in naïve CD4⁺ T cells either under TCR or P/I stimulation (Appendix Fig S5G–M). As expected, TCR- or P/I-induced NF-AT activation was specifically

inhibited in *Goliath*-deficient naïve CD4⁺ T cells as compared to WT cells, and *Goliath* deficiency abolished the obesity-promoted NF-AT activation (Fig 4A and B). Additionally, *Goliath* deficiency compromised fenofibrate- or obesity-enhanced glycolysis, as reflected by the suppressed ECAR, glycolytic flux levels, and glycolysis-related gene expression in naïve CD4⁺ T cells (Fig 4C–G and Appendix Fig S6A). In addition, *Goliath* deficiency did not affect TCA cycle and the activities of LDH and PDH in CD4⁺ T cells either under lean or obese condition (Fig 4G and Appendix Fig S6B). Therefore, these data further confirm that obesity-promoted glycolytic flux in CD4⁺ T cells is indeed dependent on the presence of Goliath protein. Accordingly, obesity failed to enhance TCR-induced cellular activation and proliferation in *Goliath*-deficient CD4⁺ T cells (Fig 4H and I). In addition, treatment with Ca²⁺ chelator EGTA or CaN inhibitor FK506 greatly suppressed cellular proliferation and abolished the difference between WT and *Goliath*-deficient naïve CD4⁺ T cells (Appendix Fig S6C), which further confirmed that Goliath-mediated CD4⁺ T cells proliferation was dependent on NF-AT signaling. However, *Goliath*-deficient naïve CD4⁺ T cells had comparable levels of basal FAO and TCR-induced OXPHOS compared with WT cells (Appendix Fig S6D–G), which further confirmed that Goliath functioned downstream of FAO. These data suggested that Goliath is indispensable for FAO-boosted glycolysis in CD4⁺ T cells during obesity.

Next, we examined the obesity-related energy metabolism and inflammation in adipose tissues and found that T cell conditional *Goliath*-deficient mice slightly decreased weight gain and exhibited lower body weight compared with WT mice under HFD condition (Appendix Fig S7A). In addition, *Goliath* deficiency in T cells slightly relieved insulin resistance and reduced blood glucose levels (Appendix Fig S7B and C). Accordingly, the oxygen consumption and energy expenditure were increased in T cell conditional

Goliath-deficient mice, while food intake, heat production, and serum triglycerides/total cholesterol (TG/TC) were comparable between WT and T cell conditional *Goliath*-deficient mice feeding with HFD (Appendix Fig S7D–H). Additionally, *Goliath* deficiency in T cells indeed compromised obesity-induced inflammation in adipose tissue, as reflecting by decreased immune cells infiltration and

inflammatory activation in adipose tissues in T cell-specific *Goliath*-deficient obese mice as compared to WT obese mice (Appendix Fig S7I). In addition, after immunization of the BM12/SJL mice with HFD or WT or *Goliath*-deficient CD4⁺ T cells from lean or obese mice, we found that the recipient mice immunized with obese WT CD4⁺ T cells produced increased antibodies and exhibited more severe

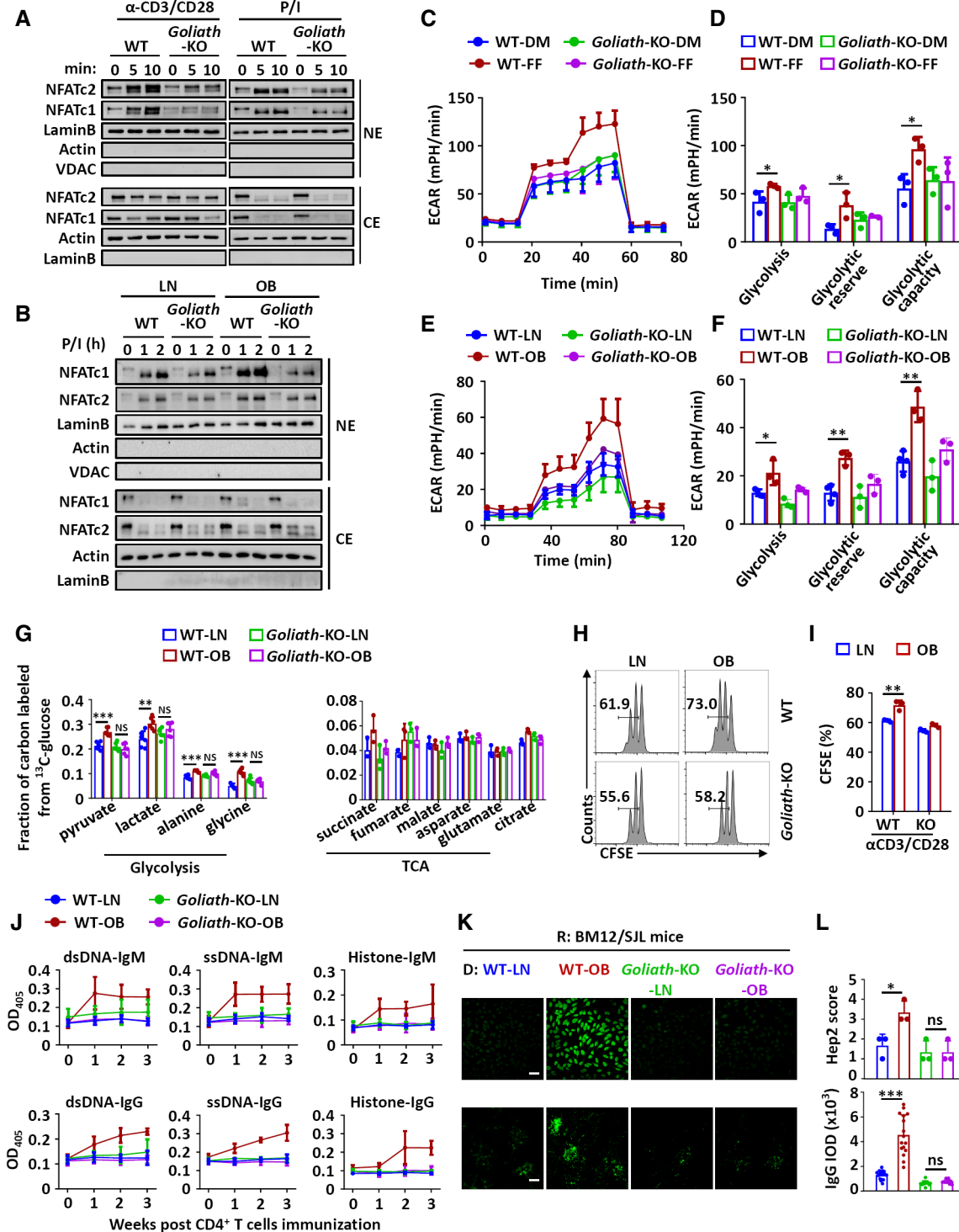


Figure 4.

Figure 4. Goliath mediates obesity-induced T cell glycolysis and inflammation.

- A, B Immunoblot analysis of cytoplasmic and nuclear NF-AT levels in WT and *Goliath*-KO naïve CD4⁺ T cells from lean (LN) or obese (OB) mice that were stimulated by α -CD3/28 (5/5 μ g/ml) or PMA/ionomycin (P/I, 10/100 ng/ml).
- C–F ECAR measurements of glycolysis in WT and *Goliath*-deficient naïve CD4⁺ T cells treated with DMSO or fenofibrate (FF, 5 μ M) (C, D), or isolated from LN or OB mice (E, F) that stimulated by α -CD3/28 (1/1 μ g/ml) for 24 h ($n = 3$, biological replicates). The statistical results are presented as bar graphs (D, F).
- G Fractions of labeled metabolites in glycolysis and TCA cycle from the [¹³C₆]glucose in CD4⁺ T cells from WT and *Goliath*-KO lean and obese mice that stimulated with α -CD3/CD28 (TCR, 1/1 μ g/ml) for 24 h ($n = 3$, biological replicates).
- H, I Proliferation analysis of splenic naïve CD4⁺ T cells from WT and *Goliath*-KO lean or obese mice upon α -CD3/28 (1/1 μ g/ml) stimulation for 3 days ($n = 3$, biological replicates). Data are presented as the representative FACS histograms (H) and statistical graphs (I).
- J–L BM12/SJL mice (recipient, R) were adoptively transferred with CD4⁺ T cells from WT and *Goliath*-KO lean or obese mice (donors, D) to induce inflammation. The anti-dsDNA, anti-ssDNA and antihistone IgG or IgM in serum were examined by ELISA (J). ANA in serum (top, scale bar: 50 μ m) and the kidney IgG deposition (bottom, scale bar: 50 μ m) were visualized using immunofluorescence ($n = 3$, biological replicates). Data are presented as Immunofluorescent images (K) and quantification bar graphs (L).

Data information: All data are representative of at least three individual experiments. Statistics, two-tailed Student's t-test; ns, not significant, * $P < 0.05$, ** $P < 0.01$, *** $P < 0.001$. Error bars represent SD.

Source data are available online for this figure.

clinical symptoms of inflammation compared with that immunized with lean WT CD4⁺ T cells. However, deletion of Goliath in CD4⁺ T cells compromised the obesity-induced exaggeration of inflammatory symptoms, characterized by the declined production of serum antibodies and decreased IgG deposition in the kidney (Fig 4J–L). These results collectively confirmed a critical role of Goliath in CD4⁺ T cells to mediate obesity-boosted inflammation through bridging obesity-elevated FAO with glycolysis.

FAO rate-limiting enzyme Cpt1a stabilizes mitochondrial Goliath

To investigate how obesity mobilizes Goliath to induce CD4⁺ T cell-mediated inflammation, we examined Goliath expression in CD4⁺ T cells under different condition or treatment. The results showed that obesity, treatment with FAO inhibitor etomoxir or *Cpt1a* deficiency did not affect the *Goliath* mRNA expression in CD4⁺ T cells (Appendix Fig S8A). However, obesity greatly increased Goliath protein level, whereas etomoxir treatment suppressed Goliath protein level and compromised obesity-induced increase of Goliath protein in CD4⁺ T cells (Fig 5A and B). In addition, the proteasome inhibitor MG132

treatment rescued etomoxir-induced decrease of Goliath protein in CD4⁺ T cells, which was also confirmed through immunoblotting in *GOLIATH*-knockdown Jurkat T cells that transfected with HA-tagged *GOLIATH* (Fig 5C–E). These data suggested obesity-elevated FAO regulated Goliath protein level through modulating its ubiquitination.

Since etomoxir directly targets Cpt1a to inhibit FAO (Lopaschuk *et al*, 1988; Klein Geltink *et al*, 2017), we speculated that obesity-elevated FAO may increase Goliath protein through Cpt1a. Consistent with its mRNA increase, the protein levels of Cpt1a, along with its transcription factor PPAR α , were markedly increased in CD4⁺ T cells from obese mice or treated with PPAR α agonist fenofibrate (Fig 5F, and Appendix Fig S8B and C). Considering that fatty acids are natural ligand to activate PPAR α -mediated transcriptional activity (Rigano *et al*, 2017), it is reasonable to speculate that obesity-induced PPAR α was activated through increased fatty acids and then promoted Cpt1a expression in CD4⁺ T cells from obese mice. Indeed, ChIP-QPCR analysis revealed that the binding activity of PPAR α in *Cpt1a* gene promoter was enhanced in CD4⁺ T cells from obese mice as compared to that in lean mice (Fig 5G).

Figure 5. FAO-induced Cpt1a stabilizes mitochondrial Goliath.

- A–D Immunofluorescence analysis of Goliath protein expression in CD4⁺ T cells from lean and obese mice as the indicated treatments. Data are presented as immunofluorescent images (A, C) and quantification bar graphs (B, D). Etomoxir (Eto), 150 μ M for 6 h; MG132, 10 μ M for the last 4 h. Scale bar: 2 μ M.
- E Immunoblot analysis of *GOLIATH* expression in *GOLIATH*-knockdown Jurkat T cells reconstituted with HA-tagged *GOLIATH* as indicated treatment. Eto, 150 μ M for 6 h; MG132, 10 μ M for 4 h.
- F Immunoblot analysis of Cpt1a and PPAR α protein expression in CD4⁺ T cells from lean and obese mice (each number represents one mouse).
- G ChIP-QPCR analysis of PPAR α binding activity in *Cpt1a* gene promoter of CD4⁺ T cells from lean and obese mice ($n = 3$, biological replicates).
- H Immunofluorescence analysis of colocalization of Goliath and Cpt1a in splenic CD4⁺ T cells from lean and obese mice. Scale bar: 2 μ m.
- I, J Immunofluorescence analysis of Goliath protein expression in CD4⁺ T cells from WT and *Cpt1a*-KO lean or obese mice. Scale bar: 2 μ m. Data are presented as immunofluorescent images (I) and quantification bar graphs (J).
- K Immunoblot analysis of Goliath protein level in *GOLIATH*-overexpressed Jurkat T cell with or without *Cpt1a* knockdown.
- L Endogenous K48-linked ubiquitination of HA-Goliath in *GOLIATH*-overexpressed Jurkat T cell with or without *Cpt1a* knockdown.
- M Endogenous ubiquitination of HA-Goliath with indicated treatment in *GOLIATH*-knockdown Jurkat T cell reconstituted with HA-tagged *GOLIATH* (WT) or Ring-truncated *GOLIATH* (Δ R).
- N Endogenous ubiquitination of HA-Goliath in *GOLIATH*-overexpressed Jurkat T cell with or without *Cpt1a* knockdown, then treated with or without etomoxir (150 μ M).
- O Immunoblot of Goliath and Cpt1a interaction in Jurkat T cells with indicated treatment. Eto: 150 μ M, MG132: 10 μ M.
- P Endogenous ubiquitination of Usp9x in WT and *Cpt1a*-deficient primary CD4⁺ T cells, then stimulated with (+) or without (–) PMA/ionomycin (P/I, 10/100 ng/ml).

Data information: All data are representative of at least three individual experiments. Statistics, two-tailed Student's t-test; ns, not significant, ** $P < 0.01$, *** $P < 0.001$. Error bars represent SD.

Source data are available online for this figure.

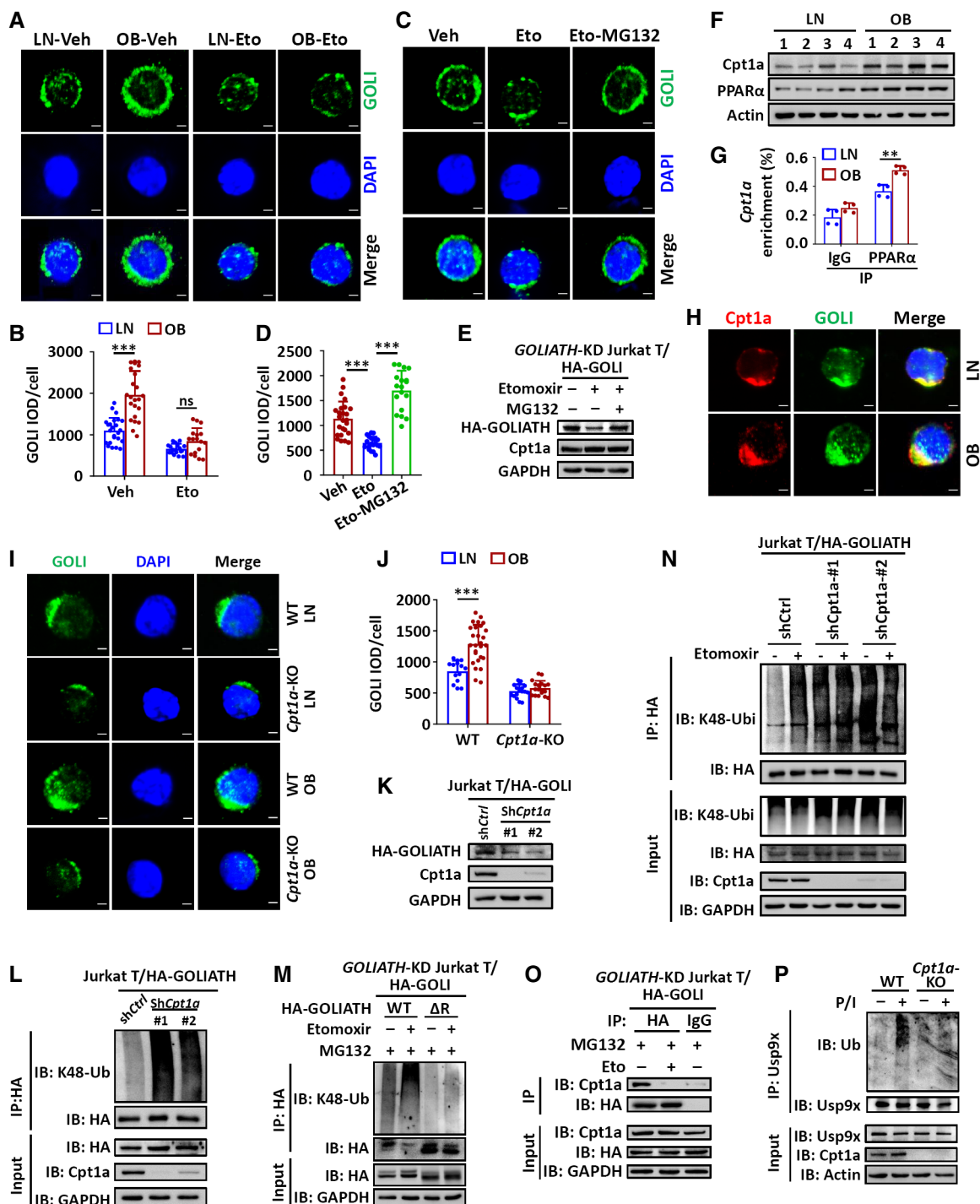


Figure 5.

Next, we found that Goliath protein colocalized with Cpt1a protein in the mitochondria of CD4⁺ T cells, which was confirmed by immunofluorescence (IF) and Co-IP analysis in 293T cells (Fig 5H, and Appendix Fig S8D and E). Similar to etomoxir treatment, deletion of Cpt1a also suppressed Goliath protein level and compromised obesity-induced increase in Goliath protein in CD4⁺ T cells (Fig 5I and J). In addition, immunoblotting also confirmed that Cpt1a knockdown decreased GOLIATH protein level in Jurkat T

cells (Fig 5K). Therefore, these data suggested that the increase in Goliath protein is dependent on FAO-induced Cpt1a during obesity.

Published study suggested that Goliath protein stability is modulated through its autoubiquitination-induced degradation (Guais *et al*, 2006). We found that Cpt1a knockdown or etomoxir treatment dramatically increased K48-linked ubiquitination of GOLIATH protein, whereas deletion of the Ring domain (E3 ligase domain) abolished GOLIATH ubiquitination in Jurkat T cells with or without

etomoxir treatment (Fig 5L and M). In addition, etomoxir treatment could not further enhance GOLIATH ubiquitination in *Cpt1a*-knockdown Jurkat T cells (Fig 5N), suggesting etomoxir-induced GOLIATH degradation is indeed through *Cpt1a*. Interestingly, Co-IP analysis revealed that *Cpt1a* interacted with multiple domains of Goliath protein, including the Ring domain, and their association was blocked by etomoxir (Fig 5O, and Appendix Fig S8F and G). These data suggested that Goliath protein wrapped *Cpt1a* to block its own E3 ligase activity, whereas etomoxir treatment blocked their association and released Goliath protein from *Cpt1a* to undergo autoubiquitination. Moreover, similar to *Goliath* deficiency, loss of *Cpt1a* also inhibited P/I-induced endogenous Usp9x ubiquitination in CD4⁺ T cells (Fig 5P). These results collectively suggested *Cpt1a* facilitated the stability of Goliath protein in mitochondria of CD4⁺ T cells during obesity.

A screened GOLIATH inhibitor suppresses obese CD4⁺ T cell-induced inflammation

To find a chemical probe capable of modulating obesity-induced inflammation, a novel sequence-based deep learning screening of chemical library was performed to look for Goliath inhibitor in our drug center (termed as DC-Gonib). Since the 3D structure of Goliath has not been determined yet, the classic structure-based screening method molecular docking is not applicable for screening inhibitors. Based on our previous work (Chen *et al*, 2020), TransformerCPI was designed to predict compound–protein interaction by using protein sequence information only (Fig 6A). After filtering nondrug-like compounds of Chemspace Library (remaining 981,244 compounds), TransformerCPI was applied to scoring compounds and top 10,000 molecules were screened out, followed by filtering Pan-assay interference compounds (PAINS), and clustering automatically. Then, 200 candidates were obtained, filtered by Lipinski rules, and selected manually. Finally, a total of 86 candidates were thus determined and experimentally evaluated (Fig 6A).

Among these 86 candidate compounds, DC-Gonib32 showed the highest inhibitory efficiency (95.3%) against TCR-induced CD4⁺ T cell proliferation (Fig 6B and C). The direct binding of Gonib32 with Goliath protein was confirmed through surface plasmon resonance and thermal shift assay (Fig 6D and Appendix Fig S8H). We found

that Gonib32 treatment did not affect the protein levels of Goliath and *Cpt1a* in Jurkat T and primary CD4⁺ T cells (Appendix Fig S8I–K). Similar to *Goliath* deficiency, Gonib32 treatment abolished TCR-induced Usp9x ubiquitination, thereby dramatically inhibiting CaN deubiquitination in primary CD4⁺ T cells (Fig 6E and F, and Appendix Fig S8L). Accordingly, the associations of CaN with Usp9x or NFATc2 were markedly suppressed in Gonib32-treated CD4⁺ T cells, which resulting in suppressed NF-AT activation and T cell proliferation (Fig 6G and H, and Appendix Fig S8M and N). More interestingly, treatment with Gonib32 eliminated obesity-boosted CD4⁺ T cell glycolysis and then cellular proliferation (Fig 6I–L and Appendix Fig S8O). Accordingly, administrated with Gonib32 suppressed the activation/proliferation *in vivo* with or without MOG immunization (Appendix Fig S8P) and compromised the obesity-induced exaggeration of proinflammatory symptoms in BM12/SJL recipient mice, characterized by compromised induction of Tfh cells and GC reaction, the declined production of serum antibodies and decreased IgG deposition in the kidney (Fig 6M–O and Appendix Fig S8Q). Moreover, Gonib32 basically mimics the phenotype of T cell with *Goliath* deficiency to improve the metabolic status of the whole body under obese condition, as reflected by slightly decreased weight gain and enhanced oxygen consumption, energy expenditure, and heat production, suggesting Gonib32 is a candidate compound showing translational potential for the treatment of obesity-related inflammation and metabolic disorders through targeting Goliath protein, and the functional validation and development of Gonib32 compound in clinic still require further detailed investigation in the future. (Appendix Fig S9A–H). Therefore, these data collectively confirmed Gonib32 was a selective inhibitor of Goliath for the treatment of obesity-induced inflammation with promising therapeutic potential.

Discussion

Obesity is a major and growing burden on public health worldwide (Swinburn *et al*, 2011; Afshin *et al*, 2017; Blüher, 2019; Schetz *et al*, 2019). Although obesity is known to be a major risk factor for many inflammatory diseases (Chaiamnuay *et al*, 2007; Versini *et al*, 2014; Kim *et al*, 2017; Van Raemdonck *et al*, 2018), the molecular mechanism controlling the etiology of obesity-

Figure 6. Screened Goliath inhibitor suppresses obesity-related inflammation.

- A Scheme of screening protocol for small-molecule inhibitors of GOLIATH protein in our drug center (DC-Gonib).
 B Proliferation inhibition analysis in murine naïve CD4⁺ T cells using the 86 screened candidate compounds, respectively ($n = 2$, biological replicates).
 C Structure of DC-Gonib32.
 D Surface plasmon resonance analysis examining the direct binding affinities of Gonib32 to purified GOLIATH protein.
 E, F Endogenous ubiquitination of Usp9x (E) and CaN (F) in primary CD4⁺ T cells treated with DMSO or Gonib32 and then stimulated with (+) or without (–) PMA/ionomycin (P/I, 10/100 ng/ml).
 G, H Immunoblot analysis of the interaction of Usp9x and CaN, NF-AT and CaN (G), and NFATc1/2 in nuclear extract (NE) and cytoplasmic extract (CE) (H) in primary CD4⁺ T cells treated with Gonib32 and then stimulated with (+) or without (–) P/I (10/100 ng/ml).
 I–L ECAR measurements of glycolysis and proliferation analysis in lean and obese naïve CD4⁺ T cells treated with DMSO or Gonib32 (2 μ M) upon α -CD3/CD28 (1/1 μ g/ml) stimulation for 24 h (ECAR) (I, J) or 3 days (proliferation) (K, L) ($n = 3$, biological replicates). The statistical results are presented as a bar graph (J, L).
 M–O BM12/SJL mice (recipient, R) were immunized with CD4⁺ T cells from lean and obese mice (donors, D), then were injected with Gonib32 (50 mg/kg) or vehicle control (5% DMSO + 95% saline) once a day for 3 weeks. Anti-dsDNA, anti-ssDNA, and anti-histone IgG or IgM in serum were measured using ELISA (M). Immunofluorescent analysis of antinuclear antibody in serum (top) and IgG deposition in the kidney (bottom) ($n = 4$ or 5, biological replicates). Data are presented as immunofluorescent images (N) and quantification bar graphs (O). All data are representative of at least three individual experiments. Statistics, two-tailed Student's *t*-test; ns, not significant, * $P < 0.5$, ** $P < 0.01$, *** $P < 0.001$. Error bars represent SD.

Source data are available online for this figure.

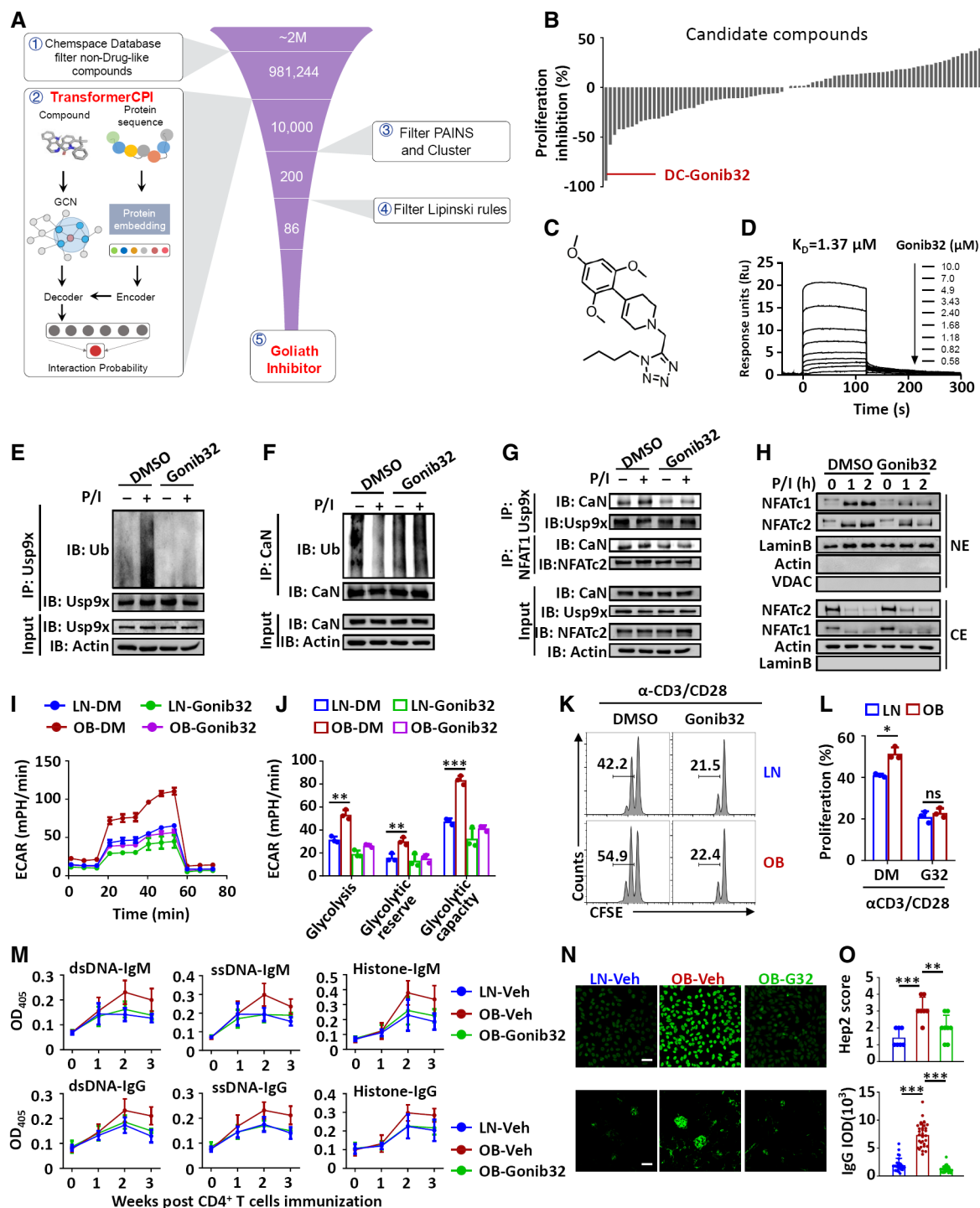


Figure 6.

induced inflammation is largely unknown. In the present study, we found that $CD4^+$ T cells from obese mice showed increased glycolysis levels along with promoted activation and proliferation, thereby enhancing their ability to induce inflammation. In addition, inhibition of glycolysis greatly abolished the activation/proliferation and proinflammatory induction difference of $CD4^+$ T cells between lean and obese mice, which established obesity as a

critical functional activator of $CD4^+$ T cells dependent on its promotion of glycolysis.

Glycolysis and FAO are two basic cellular metabolism pathways that diversely and separately modulate T cell function (Gerriets & Rathmell, 2012; MacIver *et al.*, 2013; Chapman *et al.*, 2020). However, the connection between these two pathways is not known. Obesity is associated with metabolic disorder and increased

accumulation of lipid metabolites like fatty acids (Hotamisligil, 2006; Ouchi et al, 2011). Indeed, we found that more lipid was accumulated in obese-derived resting CD4⁺ T cells, in which the genes related to fatty acids transportation, synthesis and β -oxidation were also markedly upregulated. Accordingly, the FAO level in resting CD4⁺ T cells from obese mice was enhanced as compared to that from lean mice. A plausible explanation is that long-term exposure to free fatty acids may promote the FAO level through an unknown regulatory mechanism. In addition, inhibition of FAO by using Cpt1a inhibitor or *Cpt1a*-deficient mouse greatly suppressed obesity-induced CD4⁺ T cell glycolysis and thus its activation/proliferation. These data suggested that FAO not only is critical for the generation of T memory cells as previously described but also is responsible for the enhanced CD4⁺ T cell activation/proliferation during obesity. Moreover, we found that FAO and glycolysis did not just function independently, but functioned corporately as an FAO-glycolysis axis in potentiating CD4⁺ T cell activation/proliferation in the context of obesity-associated inflammation.

It is known that induction of *in vivo* inflammation requires a certain level of T cell activation/proliferation to occur. Under lean condition, the activation/proliferation level of CD4⁺ T cells was relatively low, and thus, their ability to induce *in vivo* inflammation was also very minor, as reflected by very low levels of induction of autoantibodies in the sera and IgG deposition in the kidney of the model mice. Therefore, under lean condition, although 2-DG inhibited CD4⁺ T cell proliferation *in vitro* upon TCR stimulation, the induction difference of *in vivo* inflammation with or without 2-DG treatment was not so obvious. Accordingly, Eto treatment, *Cpt1a* or *Goliath* deficiency did not further decrease inflammation *in vivo* as well when compared to nontreated or WT cells under lean condition. By contrast, under obese condition, Cpt1a protein level was increased and thus stabilized mitochondrial Goliath protein, which further promoted the activation of CD4⁺ T cells to a level in enhancing their capability for the induction of inflammation *in vivo*, thereby resulting obvious difference of inflammation induced by WT and *Cpt1a*- or *Goliath*-KO CD4⁺ T cells. Therefore, we speculated that the protein levels of Cpt1a or Goliath need to reach a certain threshold to significantly induce glycolysis *in vitro* for inflammation induction *in vivo*.

Published studies suggested that obesity induced Th17 generation and enhanced Th17-mediated inflammatory pathologies in multiple mouse models (Jhun et al, 2012; Endo et al, 2015; Bapat et al, 2022). However, here we demonstrated that obesity promoted the pathology of Tfh-driven lupus-like inflammation. Indeed, we found that obesity specifically induced the generation of Tfh cells and thus germinal center reaction for antibody production, leading to more severe symptoms of this Tfh-driven inflammation. This difference in Th cell induction by obesity may be due to disease-context dependent, as different types of inflammation models are dominated by different lineage of Th cells. Therefore, it is highly possible that our proposed FAO-glycolysis axis could contribute to Th1 or Th17 generation in other disease models like experimental autoimmune encephalomyelitis or dermatitis.

Goliath, also known as RNF130, was first identified as a zinc-finger-motif protein in *Drosophila* (Bouchard & Côté, 1993). It is also found to be expressed in human leukocytes acting as an E3 ubiquitin ligase that is paralog of GRAIL, which is an E3 ligase in modulating the development of CD4⁺ T cell clonal anergy

(Guais et al, 2006). However, the biological function of Goliath in CD4⁺ T cells is so far unknown. Our present study found that in the context of obesity, Goliath protein was stabilized through its interaction with Cpt1a, which is upregulated through the enhanced FAO in CD4⁺ T cells from obese mice. Consequently, the stabilized Goliath activated USP9x to remove K6- and K63-linked ubiquitination of CaN, thereby promoting NF-AT activation for glycolysis metabolism. This is different from a recent study that USP16 removes the K29-linked polyubiquitin chain of CaN (Zhang et al, 2019), suggesting USP9x-mediated K6 and K63 deubiquitination of CaN is also critical for the regulation of downstream NF-AT activation and thus T cell activation/proliferation. Therefore, Goliath functions as an E3 ligase to bridge FAO with glycolysis, and this FAO-Goliath-glycolysis axis is critical for CD4⁺ T cell-mediated inflammation during obesity. Metaphorically, Goliath (the giant) is fed with fatty acid to grow bigger and bigger, Gonib32 is like the stone in King David's hand, which can effectively kill Goliath and thus save us from inflammation.

In summary, our study established Goliath as a critical mediator in bridging FAO-glycolysis axis in CD4⁺ T cells to potentiate obesity/aging-related inflammation. We also developed a selective Goliath inhibitor DC-Gonib32, which efficiently disrupted the FAO-glycolysis axis in CD4⁺ T cells and thus suppressed their ability to induce the inflammation (Appendix Fig S10). Therefore, further research and development of this inhibitor may be beneficial for the treatment of obesity/aging-related inflammatory diseases in clinic.

Materials and Methods

Mice and human samples

Cpt1a floxed mice and *Goliath* floxed mice were generated from Shanghai Research Center for Model Organisms and then were backcrossed with C57BL/6 mice at least for six generations. The C57BL/6 background *Goliath* or *Cpt1a* floxed mice were crossed with CD4-Cre mice to produce T cell conditional *Cpt1a*- or *Goliath*-knockout mice. BM12 mice were as previously described (Liu et al, 2018). In some experiment, BM12 transgenic mice were crossed with SJL transgenic mice (C57BL/6 background) to generate BM12/SJL mice. For some studies, mice were fed with either a normal diet (referred to lean mice) or a high-fat diet (HFD, 60 kcal% fat, referred to obese mice) generally from 6 to 8 weeks of age, for up to 4 months as indicated. For aged lean (AL) mice and aged obese (AO) mice, mice were fed with a normal diet for 17 months and then divided into AL (≤ 35 g) and AO (≥ 45 g) mice based on body weight as described previously (Mirsoian et al, 2014). All mice were maintained in a specific pathogen-free facility. All animal experiments were complied with all relevant ethical regulations for animal testing and research and were in accordance with protocols approved by the institutional Biomedical Research Ethics Committee, Shanghai Institute of Nutrition and Health, Chinese Academy of Sciences (IACUC number: SIBS-2019-XYC-1), according to the guidelines for Animal Experiments published by the Chinese Government.

For the analysis of metabolism-related gene expression in CD4⁺ T cells from lean and obese people, 12 normal (Body Mass Index, BMI < 25) and 21 obese (BMI > 30) people who went to Jiangsu University Affiliated Hospital for a health examination provided

blood samples. Informed consent was obtained from all study subjects prior to their inclusion in this study. The sample collection for this study was reviewed and approved by the Ethics Committee of Jiangsu University Affiliated Hospital.

Induction of *in vivo* inflammation and antibody detection

The induction of lupus-like inflammation model was as previously described (Liu *et al.*, 2018). In brief, the same amount of 7.5 million purified CD4⁺ T cells from lean and obese mice, or WT and *Goliath*-knockout lean and obese mice were intravenously injected into BM12/SJL mice. The recipient mice were intraperitoneally injected with 2-DG (200 mg/kg), DC-Gonib32 (50 mg/kg) or the same amount of vehicle (PBS for 2-DG, 5% DMSO + 95% saline for DC-Gonib32) once daily for 3 weeks, which was initiated at the first day of model induction. After 0, 1, 2, or 3 weeks later, the sera were collected to examine anti-dsDNA, anti-ssDNA, and anti-histone antibodies by enzyme-linked immunosorbent assay (ELISA). Antinuclear antibodies (ANA) were detected using Hep-2 ANA kits (INOVA Diagnostic) following the manufacturer's instructions. After sacrificing the model mice, formalin-fixed kidneys were embedded in OCT and the frozen kidney sections were stained with Alexa Fluor 488-conjugated goat anti-mouse IgG. Antibody staining was detected using a LSM880 confocal microscopy, and the fluorescence intensity was determined using Image J.

To examine CD4⁺ T cell activation/proliferation *in vivo*, aged- and sex-matched mice (8–10-week-old) were immunized s.c. with MOG₃₅₋₅₅ peptide (200 µg) mixed in CFA containing 5 mg/ml heat-killed *Mycobacterium tuberculosis* H37Ra. Pertussis toxin (200 ng/mouse) in PBS was administered intraperitoneally (i.p.) on day 0 and 2. Then, unimmunized and MOG-immunized mice were intraperitoneally injected once every two days with small-molecule inhibitor DC-Gonib32 (50 mg/kg) or same amount of vehicle (5% DMSO + 95% saline). For the *in vivo* cellular proliferation assay, 2 mg BrdU was intraperitoneally injected into the mice. Twenty-four hours later, the mice were sacrificed and the CD4⁺ T cells were collected for proliferation/activation analysis through flow cytometry.

Plasmids, antibodies, and reagents

The plasmid pCMV3-C-HA-NCV (CV013) and pCMV3-C-HA-Goliath (HG22121-CY) were purchased from Sino Biological. The plasmid pGL3-NF-AT luciferase (17870) was purchased from Addgene. The expression vector encoding Flag-Ca_v and Myc-CALM (Zhang *et al.*, 2019) was kindly provided by Dr. Jin Jin (Zhejiang University, Hangzhou, China). The expression vector encoding Flag-Usp9x (Zhu *et al.*, 2018) was kindly provided by Dr. Bin Zhao (Zhejiang University, China). The expression vector encoding Myc-Usp30 (Hou *et al.*, 2021) was kindly provided by Dr. Chengjiang Gao (Shandong University, China). The cDNAs encoding *CPT1A* and *GOLIATH* were cloned and constructed into Flag-tagged or HA-tagged pcDNA vector. *Goliath* truncated variants (27–419, 192–419, 264–419, and 305–419) were subcloned into the KpnI and XbaI sites of pCMV3-C-HA vector by PCR. All homemade and requested constructs were confirmed by DNA sequencing.

Flow cytometric antibodies for mouse CD4 (RM4-5), CD8a (53–6.7), CD44 (IM7), and CD62L (MEL-14), CD69 (H1.2F3), IFN γ (XMG1.2), IL-17A (eBio17B7), IL-4 (8D4-8), FOXP3 (FJK-16s),

CD279 (PD-1, J43), CD185 (CXCR5, SPRCL5), CD95 (Fas, 15A7), CD19 (eBio1D3 (1D3)), and CD45 (30-F11) were purchased from eBioscience. Flow cytometric antibodies for mouse CD45.1 (A20), CD45.2 (104), CD138 (281–2), GL-7 (GL7), Ki67 (16A8), and Mouse CD4⁺ T Cell Isolation Kit (480033) were purchased from Biolegend. Antibodies for NFATc1 (8032), NFATc2 (5862), Pan-Calcineurin A (2614), Ubiquitin (3933), p-ZAP70 (2701), p-LAT (3584), p-PLC γ (2821), PLC γ (2822), p-AKT (4060), p-AKT (2965), p-S6 (4858), S6 (2217), p-FOXO1 (9464), FOXO1 (2880), p-p38 (9215), p-p105 (4806), p-PI3K (4228), PI3K (4292), p-4 E-BP-1 (2855), 4 E-BP-1 (9644), p-JNK (4668), p-GSK3 (9331), HK-2 (2106), VDAC (4661), and normal rabbit IgG (2729) were purchased from Cell Signaling Technology. Antibodies for CPT1 (E-7; sc-393070), c-Myc (9E10; sc-40), Hsp60 (H-1; sc-13115), Lamin B (C-20; sc-6216), LAT (FL-233, sc-7948), AKT1 (B-1; sc-5298), p-ERK (E-4; sc-7383), ERK1 (K-23; sc-94), p38 (H-147; sc-7149), JNK (sc-474), GSK3 (sc-9166), and mouse-anti-goat IgG (HRP; sc-2354) were purchased from Santa Cruz Biotechnology. Antibodies for Usp9x (55054-1-AP), GAPDH (60004-1-Ig), and β -actin (66009-1-Ig) were purchased from Proteintech. Antibody for *Goliath* (GTX34169) was purchased from GeneTex. Antibody for Flag (A8592), Anti-phospho-Threonine Antibody (05-1923), and Anti-Phosphoserine Antibody (16-455) were purchased from Sigma-Aldrich. Antibody for HA (2013819) was purchased from Roche. Antibodies for Alexa Fluor 488-conjugated rabbit IgG (A11034), Alexa Fluor 555-conjugated mouse IgG (A31572) and Alexa Fluor Plus 488-conjugated mouse IgG (A32723), and MitoTracker[™] Deep Red FM (M22426) were purchased from Thermo Fisher Scientific. Antibodies for flow cytometry or primary antibodies for immunofluorescence were used at a dilution of 1:100; the antibodies for immunoblot or secondary antibodies for immunofluorescence were used at a dilution of 1:1,000. Annexin V FITC Apoptosis Kit (556547) and BD Cytofix/cytoperm (554722) were purchased from BD. Hep-2 ANA Kits (708100) were purchased from Inova Diagnostics. The LIVE/DEAD Fixable Violet Dead Cell Stain Kit (L34963), the CellTrace[™] Violet Cell Proliferation Kit (L34955), TRIzol reagent (15596018), RNase A (8003089), Lipofectamine RNAiMAX (13778075), Foxp3/Transcription Factor Staining Buffer Set (00-5523-600), PageRuler[™] Prestained Protein Ladder (26617), and BrdU (B23151) were purchased from Thermo Fisher Scientific. LipoFilter[™] Liposomal Transfection Reagent (HB-LF10001) was purchased from Hanbio. Antibodies for mouse CD3 (BE0001-1) and mouse CD28 (BE0015-1) were purchased from BioXcell. Goat Anti-Hamster IgG (H + L) (6060-01) was purchased from Southern Biotech. Seahorse XF Glycolysis Stress Test Kit (103020-100), Seahorse XF Cell Mito Stress Test Kit (103015-100), and Seahorse XFe96 Flux-Paks (102416-100) were purchased from Agilent. The dual-luciferase reporter assay system (E1960) was purchased from Promega. Histone from calf thymus (10223565001) and FastStart universal SYBR Green master mix (4913914001) were purchased from Roche. PrimeScript RT reagent kit (RR037A) was purchased from Takara. D-(+)-Galactose (G0750), 2-Deoxy-D-glucose (D8375), Glucose (G6152), Etomoxir sodium salt (E1905), MG132 (G2211), Fenofibrate (F6020), Cyclosporin A (239835), PMA (P1585), Ionomycin calcium salt (I0634), L-Carnitine hydrochloride (C0283), Sodium palmitate (P9767), Rotenone (R8875), FCCP (C2920), Polybrene (H9268), N-ethylmaleimide (E3876), Monoclonal Anti-HA-Agarose antibody (A2095-1ML), and Basic DMSM (D5030) were purchased from Sigma-Aldrich. Oligomycin A (A5588) and Antimycin A (B6583) were

purchased from APEX BIO. Tacrolimus (FK506; S5003) was purchased from SelleckChem. 60 kcal% Fat (D12492) was purchased from Research Diets. Cell-Tak™ (354240) was purchased from CORNING. Penicillin–Streptomycin (15140-122) and GlutaMAX™ Supplement (35050-061), and Sodium pyruvate (11360070) were from Gibco. DMEM/High Glucose (SH30243.01) and RPMI Medium Modified (SH30809.01), 2-Mercaptoethanol (21985023) were from Hyclone. RPMI 1640 Medium (no glucose, no glutamine; 01-101-1A) and Certified Fetal Bovine Serum (FBS; 04-001-1A) were from Biological Industries. Protease Inhibitor Cocktail (B14001) and Phosphatase Inhibitor Cocktail (B15001) were from Bimake. YeaRed Nucleic Acid Gel Stain (10202ES76) and BSA (fatty acid free) (36104ES25) were from YEASEN. Anti-Fade Mounting Medium (E675011), Puromycin (A610593), BSA (A602440), and DAPI dihydrochloride (A606584) were from Sangon Biotech. BODIPY (GC42959) was from GLPBIO. Immobilon Western chemiluminescent HRP substrate (SQ201) was from Epizyme. TIANprep Mini Plasmid Kit (DP103-03), DNA marker II (MD102), and DNA marker III (MD103) were from TIANGEN. Fluo-3 AM (14960) was from Cayman Chemical. Pertussis toxin (180) was from List Biological Laboratories. *Mycobacterium tuberculosis* H37Ra (231141) was from Difco.

Cell culture, transfection, gene silencing, and overexpression

All the cell lines that used were kept in our laboratory and tested for the negative mycoplasma contamination. The human embryo kidney 293T cells were cultured with DMEM containing 10% FBS. The human Jurkat T cells and murine primary CD4⁺ T cells were cultured with RPMI 1640 medium supplemented with 10% FBS. For knockdown of *Cpt1a*, *Goliath*, and *Usp9x* or overexpression of *Goliath* in Jurkat T cells, lentiviral particles were prepared by transfecting HEK293T cells with pLKO.1 lentiviral vectors encoding shRNA or pCDH-MCS-copGFP encoding *Goliath* along with packaging plasmids psPAX2 and pMD2.G with Lipofiter™ Transfection Reagent (Hanbio) as per manufacturer's instructions. The supernatant was harvested at 48 h after transfection. For transduction of Jurkat T cells, lentivirus was added to infect Jurkat T cells in the presence of polybrene (8 µg/ml), followed by selection using puromycin (1 µg/ml) for 24 h or sorting with flow cytometric based on GFP expression. The knockdown efficiency was examined by qRT–PCR and immunoblotting. The sequences of shRNA/siRNA for specific gene knockdown are listed in Appendix Table S1.

For *Goliath* overexpression or *Usp9x* knockdown in primary CD4⁺ T cells, CD4⁺ T cells were stimulated with anti-CD3 and anti-CD28 for 16–18 h and then infected with the supernatant containing fresh retrovirus produced by transfecting Plat-E cells with the indicated plasmids. The infected T cells were spun for 1.5 h at 1,800 g in the presence of polybrene (8 µg/ml) and were cultured at 37°C for an additional 2–6 h before being resuspended in RPMI 1640 medium supplemented with 10% FBS.

T cell activation and proliferation

Murine CD4⁺ T cells were isolated from the spleen and peripheral lymph nodes of mice with Mouse CD4⁺ T cell isolation kit (Biolegend). Naïve CD4⁺ T cells were further purified by the flow cytometric cell sorting based on CD4⁺CD44^{lo}CD62L^{hi}. For

immunoblotting, isolated naïve CD4⁺ T cells were activated with anti-CD3 and anti-CD28 (crosslinked with anti-hamster IgG) on a vortex shaker at 37°C for 5 or 10 min. In addition, isolated naïve CD4⁺ T cells were stimulated with PMA (phorbol 12-myristate 13-acetate, 10 ng/ml) and Ionomycin (100 ng/ml) for 1 or 2 h. For qRT–PCR, naïve CD4⁺ T cells were stimulated with plate-bound anti-CD3 (1 µg/ml) and anti-CD28 (1 µg/ml) as indicated times. For T cell proliferation assay (CFSE), naïve T cells were labeled in 5 µM CFSE in 37°C and washed with PBS. The cells were normalized and cultured in 96-well plates with plate-coated anti-CD3 (1 µg/ml) and anti-CD28 (1 µg/ml) for 72 h and then were subjected to flow cytometry analyses.

Flow cytometry (FACS)

For analysis of surface markers, cells were stained in PBS with 2% FBS on ice for 30 min. For intracellular cytokines staining, cells were stimulated with PMA/ionomycin (200/500 ng/ml) and monensin for 4 h and followed by staining with fixation/permeabilization buffer solution according to the manufacturer's protocol (BD Biosciences). Intranuclear staining was performed with fixation/permeabilization buffer solution according to the manufacturer's protocol (eBioscience). To stain for neutral lipids, splenic cells or isolated CD4⁺ T cells were incubated with BODIPY (10 µM, GLPBIO) diluted in PBS for 15 min at 37°C. After BODIPY staining, cells were stained with the flow cytometry antibodies. Data collection was performed on a Beckman Gallios cytometer and analyzed using FlowJo software. For the gating strategy, FSC/SSC is initial applied and then used the antibodies with specific fluorochrome to make the subsequent gates. All the samples in the same experiments and comparisons were gated under the same parameters.

Immunoblot and immunoprecipitation

Cells were lysed and whole-cell lysates or subcellular extracts were prepared for immunoprecipitation or immunoblotting. For preparation of nuclear versus cytosolic fractions, cells were lysed in Buffer B lysis buffer and left on ice for 30 min. After spinning at 16,100 g for 3 min, the supernatants were transferred into a new tube as cytosol fraction. The nuclear pullets were washed with Buffer C on ice for 5 min and centrifuged at 16,100 g to remove wash buffer. These pullets were shaken vigorously on a vortex shaker at 4°C for 1 h. Following centrifugation at 16,100 g for 3 min, the supernatants were nuclear extracts. For immunoprecipitation, cells were lysed in RIPA buffer with protease inhibitors on ice for 30 min. The whole-cell lysates were incubated with desired antibodies overnight, and protein A/G magnetic beads were added to pull down target protein. The samples were resolved by SDS–PAGE, transferred to nitrocellulose membranes, blocked with 5% nonfat milk, incubated with specific primary antibody and horseradish peroxidase-conjugated secondary antibody, and detected by ECL.

Ubiquitination assay

The *in vivo* ubiquitination assay was performed as described previously (Pei et al., 2021). In brief, primary CD4⁺ T cells with different treatment or from different mice were stimulated with α-CD3/28

(TCR, 5/5 $\mu\text{g/ml}$) or PMA/Ionomycin (P/I, 10/100 ng/ml) or not for different time. Then cells were lysed with cell lysis RIPA buffer (50 mM Tris-HCl, pH 7.4, 150 mM NaCl, 1% NP-40, 0.5% sodium deoxycholate, and 1 mM EDTA) containing protease inhibitor and *N*-ethylmaleimide (Sigma-Aldrich). After saving some cell extracts for input analysis, the remaining cell extracts were added to SDS to a final concentration of 1% and then were boiled at 100°C for 5 min, which will dissociate all the potential proteins under such denaturing conditions. The boiled cell extracts were diluted with RIPA buffer until the SDS concentration was 0.1%, precleaned with protein A/B-coupled agarose beads, and then incubated with specific immunoprecipitation antibody on a shaker under denaturing conditions (0.1% SDS) at 4°C overnight. The next day, the immunoprecipitated proteins were collected by incubation with protein A/B-coupled agarose beads on a shaker at 4°C for 2 h; washed with RIPA buffer containing protease inhibitors, PMSF, and *N*-ethylmaleimide; boiled at 100°C for 5 min; and then loaded to run SDS-PAGE. The immunoprecipitates were immunoblotted with anti-ubiquitin or the indicated antibodies.

Immunofluorescence and confocal microscopy

For analysis of GOLIATH or Cpt1a expression, freshly isolated CD4⁺ T cells were seeded in 96-well plates, and then left untreated or treated with Etomoxir (150 μM) for 6 h in the presence or absence of MG132 (10 μM) for the last 4 h, or treated with DC-Gonib32 (2 μM) for 12 h. The cells (2×10^5) were thrown onto the slides by using cytocentrifuge, fixed with 4% paraformaldehyde (PFA) for 20 min, permeabilized by 0.2% Triton X-100 for 5 min and blocked with 3% BSA for 1 h. Then, cells were stained with indicated antibodies or Mitotracker, followed by fluorescent-conjugated secondary antibodies, and were counterstained with DAPI. The stained cells were imaged on a LSM880 (Carl Zeiss) outfitted with a Plan-Apochromat 63 \times oil immersion objective lenses (Carl Zeiss). For analysis of fluorescence intensity, the images were processed in Image J. For each group, at least 30 images were calculated using integrated intensity normalized to cell number with the same function parameters.

Extracellular flux analysis

Extracellular acidification rates (ECAR) and oxygen consumption rates (OCR) were measured using an XF²⁴ or an XF⁹⁶ Extracellular Flux Analyzer (Seahorse Bioscience). One day before the assay, Seahorse Bioscience utility plate was added calibrant (pH 7.4) and then placed sensor cartridge on top of the utility plate and stored at 37°C without CO₂ overnight. On the contrary, cell culture plates were plated with Cell-Tak and incubated overnight in 4°C.

For ECAR assay, naïve CD4⁺ T cells were subjected to anti-CD3 (1 $\mu\text{g/ml}$) and anti-CD28 (1 $\mu\text{g/ml}$) stimulation with the indicated treatment for 24 h. Then, cells were resuspended in ECAR assay media supplemented with 2 mM L-Glutamine (Gibco; pH 7.4) and plated in XF-96 plates at a density of 2×10^5 cells/well. ECAR was measured in basal conditions and following treatment with following agents: glucose (25 mM); the ATP synthase inhibitor oligomycin (5 μM); glucose analog 2-DG (100 mM). Experiments with the Seahorse system were done with the following assay conditions: 3 min of mixture; 3 min of waiting; and 3 min of measurement.

Glycolysis was calculated as the difference between the glucose-stimulated ECAR and basal ECAR. Glycolytic capacity was calculated as the difference between the oligomycin-stimulated ECAR and basal ECAR. Glycolytic reserve was calculated as the difference of the glycolytic capacity to glycolysis level.

For OCR assay, cells were resuspended in OCR assay media supplemented with 10 mM glucose, 2 mM L-Glutamine (Gibco), and 1 mM sodium pyruvate (Gibco; pH 7.4) and plated in XF-96 plates at a density of 2×10^5 cells/well. OCR was measured in basal conditions and following treatment with following agents: the ATP synthase inhibitor oligomycin (5 μM); the protonophore carbonyl cyanide-4-(trifluoromethoxy) phenylhydrazone (FCCP; 1.5 μM) to uncouple mitochondria; the mitochondrial complex I inhibitor rotenone (1 μM) and the mitochondrial complex III inhibitor antimycin A (100 nM). Basal respiration was calculated as the difference between basal OCR and rotenone/antimycin-inhibited OCR. Maximal respiration was calculated as the difference between FCCP-stimulated OCR and rotenone/antimycin-inhibited OCR. Respiratory reserve was calculated as the difference between maximal respiration and basal respiration.

For the cellular basal fatty acid β -oxidation (FAO) analysis, fresh isolated naïve CD4⁺ T cells were resuspended with FAO buffer (111 mM NaCl, 4.7 mM KCl, 1.25 mM CaCl₂, 2 mM MgSO₄, 1.2 mM NaH₂PO₄, 2.5 mM glucose, 0.5 mM carnitine, and 5 mM HEPES, pH 7.4). Resuspended cells were plated in 24-well microplate (Agilent) at 1.2×10^6 cells/well and were incubated in at 37°C in a humidified atmosphere without CO₂ for 30 min, then added with FAO substrate Palmitate-BSA or BSA, and measured as above-mentioned OCR assay.

Measurement of metabolic flux by gas chromatography–mass spectrometry (GC–MS)

The labeling 1640 medium composed of 1 g/l [U-¹³C₆]glucose, 1 g/l D-glucose, 10% (v/v) FBS, 1 mM pyruvate, unlabeled 2 mM L-glutamine and 1% (v/v) penicillin–streptomycin. CD4⁺ T cells cultured in labeling 1,640 medium were stimulated with anti-CD3 (1 $\mu\text{g/ml}$) and anti-CD28 (1 $\mu\text{g/ml}$) for 24 h. CD4⁺ T cells were collected at a density of approximately 1×10^7 cells per sample. Nonsugar metabolites were derivatized for GC/MS analysis and followed a previously published protocol (Nanchen *et al.*, 2007). Briefly, cells were grinded in liquid nitrogen and resuspended in 1 ml cold (–40°C) 50% aqueous methanol containing (100 μM norvaline) as an internal standard and inserted in dry ice for 30 min and then thawed samples on ice. Next added 0.4 ml chloroform and vortexed for 30 s before centrifugation for 10 min at 18,407 g (4°C), transferred supernatant to new 1.5 ml tubes to evaporate, and stored at –80°C before analysis. Metabolites were derivatized for GC/MS analysis as follows: First, 70 μl of pyridine was added to the dried pellet and incubated for 20 min at 80°C. After cooling, 30 μl of *N*-tert-butyltrimethylsilyl-*N*-methyltrifluoroacetamide was added and samples were reincubated for 60 min at 80°C before centrifugation for 10 min at 18,407 g (4°C). The supernatant was transferred to an autosampler vial for GC/MS analysis. A Shimadzu QP-2010 Ultra GC–MS was programmed with an injection temperature of 250°C injection and injected with 1 μl of sample. GC oven temperature started at 110°C for 4 min, rising to 230°C at 3°C/min and to 280°C at 20°C/

min with a final hold at this temperature for 2 min. GC flow rate with helium carrier gas was 50 cm/s. The GC column used was a 20 m × 0.25 mm × 0.25 mm Rxi-5 ms. GC–MS interface temperature was 300°C, and (electron impact) ion source temperature was set at 200°C, with 70 V ionization voltage. The mass spectrometer was set to scan *m/z* range 50–800, with 1 kV detector. GC/MS data were analyzed to determine isotope labeling. To determine ¹³C labeling, the mass distribution for known fragments of metabolites was extracted from the appropriate chromatographic peak. These fragments contained either the whole carbon skeleton of the metabolite, or lacked the alpha carboxyl carbon, or (for some amino acids) contained only the backbone minus the side chain (van Winden *et al*, 2002). For each fragment, the retrieved data comprised mass intensities for the lightest isotopomer (without any heavy isotopes, M0) and isotopomers with increasing unit mass (up to M6) relative to M0. These mass distributions were normalized by dividing by the sum of M0 to M6 and corrected for the natural abundance of heavy isotopes of the elements H, N, O, Si, and C, using matrix-based probabilistic methods as described (Portnoy *et al*, 2010), and implemented in MATLAB. Labeling results are expressed as average fraction of the particular compound that contains isotopic label from the particular precursor.

Luciferase reporter assay and gene knockdown in HEK293T cells

For knockdown of E3 ligases or DUBs located in mitochondria, siRNA targeting the indicated genes and negative control were transfected into HEK293T cells with Lipofectamine RNAiMAX (Invitrogen). After 16 h, NF-AT luciferase reporter was transfected into cells using Lipofilter™ Transfection Reagent (Hanbio). PMA/ionomycin were added 3 h before cells harvesting. NF-AT transcriptional activity was measured with Dual-Luciferase Reporter Assay System (Promega), and the relative light unit of chemiluminescence was measured by LB 9508 Lumat3 (Berthold Technologies). The siRNA sequences for targeting specific genes are listed in Appendix Table S1.

RNA-sequencing analysis

Fresh splenic CD4⁺ T cells were isolated from lean/obese mice. These T cells were used for total RNA isolation using TRIzol (Thermo) and subjected to RNA-seq analysis. RNA sequencing was performed by BGI Tech Solutions. The raw transcriptome was mapped to a reference genome (GRCm38/mm10) by using Bowtie. Gene expression levels were quantified by the RSEM software package. Differentially genes were analyzed using the DAVID bioinformatics platforms.

Real-time quantitative RT–PCR (qRT–PCR)

Total RNA was extracted using TRIzol reagent and subjected to cDNA synthesis using PrimeScript RT Reagent Kit (Takara). qRT–PCR was performed on QuantStudio 7 Flex Real-Time PCR System (Applied Biosystems) with SYBR Green Master Mix (Novoprotein). The expression of individual genes was calculated by a standard curve method and normalized to the expression of *Actb*. The gene-specific PCR primers (all for mouse genes) are shown in Appendix Table S2.

Mass spectrometry (MS)

For identification of the DUB binding to both Goliath and CaN, HA-Goliath and Flag-CaN expression plasmids were transiently transfected into HEK293T cells using Lipofilter™ Transfection Reagent (Hanbio), respectively. After 48 h, cells were harvested and lysed with RIPA buffer containing protease inhibitors. Whole-cell lysates of HEK293T cells that transfected with HA-Goliath or Flag-CaN were immunoprecipitated with the anti-HA- or Flag-conjugated agarose beads on a shaker at 4°C for overnight, then were washed with cell lysis buffer, eluted with Glycine-Tris–HCl buffer (pH 2.5), and then sent to process with MS analysis of protein–protein interaction.

ChIP-QPCR assay

Chromatin immunoprecipitation (ChIP) assay procedure was as previously described (Yu *et al*, 2019; Zhu *et al*, 2020). Briefly, isolated CD4⁺ T cells (about 2 × 10⁷ cells) were fixed with 1% formaldehyde (Sigma-Aldrich) at room temperature for 10 min in 10 ml media, followed by quenching with 125 mM glycine. Nuclear extracts were sonicated with Covaris E220 for 660 s. After pre-clearing with normal IgG for 1 h, the sonicated cell lysates were immunoprecipitated with the PPARα antibody overnight on an incubator at 4°C. The next day, protein A/G magnetic beads were added and cell lysates were incubated on an incubator for another 2 h. After washing with buffers, chromatin was eluted from the protein/DNA complex and digested with proteinase K and RNase A at 65°C overnight to reverse cross-links. The freed DNA was purified with AxyPrep PCR cleanup kit (Axygen) and subjected to quantitative PCR analysis by using SYBR Green master mix. All the sequences of primers for ChIP-QPCR are shown in Appendix Table S2.

Screening of small-molecule inhibitors of Goliath

The details of TransformerCPI model are available in our previous work (Chen *et al*, 2020). The 252,124 compound–protein interactions with binary labels (117,513 active and 134,611 inactive) were collected from ChEMBL 23, which were then used as training and testing set of TransformerCPI model. TransformerCPI was trained by the RADam optimizer with learning rate of 1e-5 and weight decay of 1e-3. Batch size was selected to ensure the longest protein sequence fit into GPU memory and was 8. We employed gradient accumulation technique to expand the actual batch size to 64. First, the optimized TransformerCPI model was used for the further screening of 981,244 compounds from ChEMBL Library. Then, top 10,000 compounds were selected, filtered PAINS structures, and clustered automatically, and 200 representative compounds were obtained. Finally, the 200 representative molecules were filtered by Lipinski rules and selected manually. A total of 86 candidates were thus determined and purchased for further investigation.

Protein expression and purification

GOLIATH (residues 1–304) with a C-terminal His₈-Flag-tag were subcloned into the pcDNA3.1 vector. Proteins were expressed in Expi-293F (Invitrogen) using Expifectamine transfection reagent according to the manufacturer's instructions. Cells were collected 3 days after infection. Proteins were first captured by Ni²⁺-

Sepharose 6 Fast Flow resin (GE healthcare) and then further purified by gel filtration chromatography with a Superdex S200 column (GE healthcare). The purified protein was concentrated and stored in buffer (20 mM HEPES pH 7.5, 150 mM NaCl and 1 mM TCEP) at -80°C .

Glucose- and insulin-tolerance tests (GTT and ITT)

Singly caged mice were deprived of food for 6 h before testing. For glucose-tolerance tests (GTT), mice were weighed and injected with 1 g/kg D-glucose. For insulin-tolerance tests (ITT), mice were weighed and injected with 0.75 U/kg of human recombinant insulin. For both tests, blood glucose levels were measured using the Glucose Meter by tail bleeding 0, 15, 30, 60, 90, and 120 min after injection of glucose or insulin.

Metabolic cage study

For the indirect calorimetry study, we housed and monitored mice for 4 days in metabolic cages (Comprehensive Lab Animal Monitoring System: CLAMS-16, Columbus Instruments) at 22°C . Mice were housed individually and maintained on a 12 h light–dark cycle with lights on from 6:00 to 18:00. The first 2 days were used for mice to acclimatize to the system; then, we analyzed oxygen consumption (VO_2), carbon dioxide production (VCO_2), and heat generation during the next day. The oxygen consumption (ml/kg/h) and heat generation (kcal/kg/h) of each mouse were calculated according to its body weight.

Calcium flux analysis

CD4^+ T cells were labeled with 5 μM Fluo-3 Acetoxymethyl ester (Fluo-3 AM; Molecular Probe) and incubated at 37°C for 60 min. For determination of baseline, calcium signals were recorded for 90 s by flow cytometry without stimulation. After 90 s, PMA/Ionomycin (10/100 ng/ml) were added and calcium fluxes were measured for a total of 4 min. Calcium signals were recorded on a Gallios (Beckman).

Surface plasmon resonance (SPR)

SPR binding assay was performed using a Biacore T200 instrument (GE Healthcare). The purified Goliath protein was covalently immobilized onto CM5 sensor chip (GE Healthcare) by a standard amine-coupling procedure in 10 mM sodium acetate (pH 4.5) with running buffer HBS (50 mM HEPES (pH 7.4), 150 mM NaCl). DC-Gonib32 was serially diluted and injected onto the sensor chip at a flow rate of 30 $\mu\text{l}/\text{min}$ for 120 s (contact phase), followed by 120 s of buffer flow (dissociation phase). The equilibrium dissociation constant (K_D) value was derived using the Biacore T200 Evaluation software (version 1.0, GE Healthcare).

Cellular thermal shift assay (CETSA)

HEK293T cells transfected with Flag-Goliath for 48 h were collected and lysed in 20 mM Tris (pH 7.5), 150 mM NaCl and 1% Triton X-100. Then, 50 μM Gonib32 or DMSO was added to the supernatant and incubated at 25°C for 30 min. After denaturing at various

temperatures for 3 min on temperature gradient PCR instrument (Eppendorf), samples were centrifuged at 20,000 g for 30 min at 4°C and the supernatants were analyzed by Western blot. All samples containing 1 \times loading buffer (Beyotime, P0015) were denatured at 100°C for 5 min and separated by 8% SDS–PAGE and then transferred to nitrocellulose membranes. Membranes were blocked with Blocking buffer (Beyotime, P0252) and then incubated with anti-Flag (Cell Signaling Technology, 14793) or anti- β -Tubulin (Cell Signaling Technology, 15115) primary antibodies overnight at 4°C , followed by incubation with HRP-conjugated anti-rabbit secondary antibody (Promega, W4011) for 1 h at room temperature. Lastly, the immune complexes were detected with ECL kit (Meilun, MA0186) and visualized using GenGnome XRQ NPC.

Statistical analysis

No statistical methods were used to determine the sample size. The experiments were randomized, and the investigator was not blinded. The data are shown as mean \pm SD, and unless otherwise indicated, all the presented data were the representative results of at least three biologically independent repeats. Statistical analysis was performed by using GraphPad Prism 8 (GraphPad Software), and the statistics were analyzed by a two-tailed Student's *t*-test or one-way or two-way ANOVA as indicated. Differences were considered to be significant at $P < 0.05$ and are indicated by *, those at $P < 0.01$ are indicated by **, and those at $P < 0.001$ are indicated by ***.

Data availability

The RNA-sequencing data have been deposited in the Gene Expression Omnibus (accession no. GSE188864, <https://www.ncbi.nlm.nih.gov/geo/query/acc.cgi?acc=GSE188864>). All other data supporting the findings of this study are available from the corresponding authors on reasonable request.

Expanded View for this article is available [online](#).

Acknowledgements

We would like to thank Drs. Jin Jin, Bin Zhao (Zhejiang University, China), Chengjiang Gao (Shandong University, China), Qirong Ding, and Yu Li (Shanghai Institute of Nutrition and Health, Chinese Academy of Sciences, China) for their kind helps in this study. We also appreciate the assistance from the personnel of animal and platform core facilities in Shanghai Institute of Nutrition and Health, Chinese Academy of Sciences. This research was supported by the grants from the National Natural Science Foundation of China (82030041, 82001657), the Strategic Priority Research Program of the Chinese Academy of Sciences (XDB39030300), the National Key R&D Program of China (2018YFA0107201, 2018YFA0902703), the programs from Science and Technology Commission of Shanghai Municipality (20XD1424600, 21140905000), China Postdoctoral Science Foundation (2021M702163, 2021M700160, 2021M693272), and CAS Key Laboratory of Tissue Microenvironment and Tumor.

Author contributions

SH and JY designed and performed the experiments, prepared the figures, and wrote part of the manuscript; SZ and LC contributed to the screening and

enzymatic activity analysis of GOLIATH inhibitors; YW, SP, QZ and JX contributed to the experiments; YT and HY contributed to the metabolic flux analysis; NZ and CWD generated *Cpt1a*-flox mice; CM provided the human blood samples. MZ supervised the screening and analysis of GOLIATH inhibitors, prepared the figures and wrote the manuscript; YX initiated, designed and supervised this study, prepared the figures and wrote the manuscript.

Disclosure and competing interests statement

YX, MZ, SH, SZ, LC, and JY have filed a patent application regarding the generation and application in inflammatory diseases of DC-Gonib32 and its derivatives. The authors declare that they have no conflict of interest.

References

- Afshin A, Forouzanfar MH, Reitsma MB, Sur P, Estep K, Lee A, Marczak L, Mokdad AH, Moradi-Lakeh M, Naghavi M *et al* (2017) Health effects of overweight and obesity in 195 countries over 25 years. *N Engl J Med* 377: 13–27
- Bapat SP, Whitty C, Mowery CT, Liang Y, Yoo A, Jiang Z, Peters MC, Zhang LJ, Vogel I, Zhou C *et al* (2022) Obesity alters pathology and treatment response in inflammatory disease. *Nature* 604: 337–342
- Blüher M (2019) Obesity: global epidemiology and pathogenesis. *Nat Rev Endocrinol* 15: 288–298
- Bouchard ML, Côté S (1993) The *Drosophila melanogaster* developmental gene *g1* encodes a variant zinc-finger-motif protein. *Gene* 125: 205–209
- Chaiamnuay S, Bertoli AM, Roseman JM, McGwin G, Apte M, Durán S, Vilá LM, Reveille JD, Alarcón GS (2007) African-American and Hispanic ethnicities, renal involvement and obesity predispose to hypertension in systemic lupus erythematosus: results from LUMINA, a multiethnic cohort (LUMINAXLV). *Ann Rheum Dis* 66: 618–622
- Chang CH, Curtis JD, Maggi LB Jr, Faubert B, Villarino AV, O'Sullivan D, Huang SC, van der Windt GJ, Blagih J, Qiu J *et al* (2013) Posttranscriptional control of T cell effector function by aerobic glycolysis. *Cell* 153: 1239–1251
- Chapman NM, Boothby MR, Chi H (2020) Metabolic coordination of T cell quiescence and activation. *Nat Rev Immunol* 20: 55–70
- Chen L, Tan X, Wang D, Zhong F, Liu X, Yang T, Luo X, Chen K, Jiang H, Zheng M (2020) TransformerCPI: improving compound-protein interaction prediction by sequence-based deep learning with self-attention mechanism and label reversal experiments. *Bioinformatics* 36: 4406–4414
- Cox AJ, West NP, Cripps AW (2015) Obesity, inflammation, and the gut microbiota. *Lancet Diabetes Endocrinol* 3: 207–215
- Endo Y, Asou HK, Matsugae N, Hirahara K, Shinoda K, Tumes DJ, Tokuyama H, Yokote K, Nakayama T (2015) Obesity drives Th17 cell differentiation by inducing the lipid metabolic kinase, ACC1. *Cell Rep* 12: 1042–1055
- Frauwirth KA, Riley JL, Harris MH, Parry RV, Rathmell JC, Plas DR, Elstrom RL, June CH, Thompson CB (2002) The CD28 signaling pathway regulates glucose metabolism. *Immunity* 16: 769–777
- Gerriets VA, Rathmell JC (2012) Metabolic pathways in T cell fate and function. *Trends Immunol* 33: 168–173
- Guais A, Siegrist S, Solhonne B, Jouault H, Guellaen G, Bulle F (2006) h-Goliath, paralog of GRAIL, is a new E3 ligase protein, expressed in human leukocytes. *Gene* 374: 112–120
- Hotamisligil GS (2006) Inflammation and metabolic disorders. *Nature* 444: 860–867
- Hou J, Han L, Zhao Z, Liu H, Zhang L, Ma C, Yi F, Liu B, Zheng Y, Gao C (2021) USP18 positively regulates innate antiviral immunity by promoting K63-linked polyubiquitination of MAVS. *Nat Commun* 12: 2970
- Huang X, Hao S, Liu J, Huang Y, Liu M, Xiao C, Wang Y, Pei S, Yu T, Xu J *et al* (2021) The ubiquitin ligase Peli1 inhibits ICOS and thereby Tfh-mediated immunity. *Cell Mol Immunol* 18: 969–978
- Jhun JY, Yoon BY, Park MK, Oh HJ, Byun JK, Lee SY, Min JK, Park SH, Kim HY, Cho ML (2012) Obesity aggravates the joint inflammation in a collagen-induced arthritis model through deviation to Th17 differentiation. *Exp Mol Med* 44: 424–431
- Kaminski DA, Randall TD (2010) Adaptive immunity and adipose tissue biology. *Trends Immunol* 31: 384–390
- Kim SJ, Chen Z, Essani AB, Elshabrawy HA, Volin MV, Fantuzzi G, McInnes IB, Baker JF, Finn P, Kondos G *et al* (2017) Differential impact of obesity on the pathogenesis of RA or preclinical models is contingent on the disease status. *Ann Rheum Dis* 76: 731–739
- Klein Geltink RI, O'Sullivan D, Corrado M, Bremser A, Buck MD, Buescher JM, Firat E, Zhu X, Niedermann G, Caputa G *et al* (2017) Mitochondrial priming by CD28. *Cell* 171: 385–397
- Liu J, Huang X, Hao S, Wang Y, Liu M, Xu J, Zhang X, Yu T, Gan S, Dai D *et al* (2018) Peli1 negatively regulates noncanonical NF- κ B signaling to restrain systemic lupus erythematosus. *Nat Commun* 9: 1136
- Lochner M, Berod L, Sparwasser T (2015) Fatty acid metabolism in the regulation of T cell function. *Trends Immunol* 36: 81–91
- Lopaschuk GD, Wall SR, Olley PM, Davies NJ (1988) Etomoxir, a carnitine palmitoyltransferase I inhibitor, protects hearts from fatty acid-induced ischemic injury independent of changes in long chain acylcarnitine. *Circ Res* 63: 1036–1043
- Macian F (2005) NFAT proteins: key regulators of T-cell development and function. *Nat Rev Immunol* 5: 472–484
- Macintyre AN, Gerriets VA, Nichols AG, Michalek RD, Rudolph MC, Deoliveira D, Anderson SM, Abel ED, Chen BJ, Hale LP *et al* (2014) The glucose transporter Glut1 is selectively essential for CD4 T cell activation and effector function. *Cell Metab* 20: 61–72
- MacIver NJ, Michalek RD, Rathmell JC (2013) Metabolic regulation of T lymphocytes. *Annu Rev Immunol* 31: 259–283
- Mauro C, Smith J, Cucchi D, Coe D, Fu H, Bonacina F, Baragetti A, Cermentati G, Caruso D, Mitro N *et al* (2017) Obesity-induced metabolic stress leads to biased effector memory CD4(+) T cell differentiation via PI3K p110 δ -Akt-mediated signals. *Cell Metab* 25: 593–609
- McLaughlin T, Ackerman SE, Shen L, Engleman E (2017) Role of innate and adaptive immunity in obesity-associated metabolic disease. *J Clin Invest* 127: 5–13
- Mirsoian A, Bouchlaka MN, Sckisel GD, Chen M, Pai CC, Maverakis E, Spencer RG, Fishbein KW, Siddiqui S, Monjazeb AM *et al* (2014) Adiposity induces lethal cytokine storm after systemic administration of stimulatory immunotherapy regimens in aged mice. *J Exp Med* 211: 2373–2383
- Mishra AK, Dubey V, Ghosh AR (2016) Obesity: an overview of possible role(s) of gut hormones, lipid sensing and gut microbiota. *Metabolism* 65: 48–65
- Nanchen A, Fuhrer T, Sauer U (2007) Determination of metabolic flux ratios from 13C-experiments and gas chromatography-mass spectrometry data: protocol and principles. *Methods Mol Biol* 358: 177–197
- Ouchi N, Parker JL, Lugus JJ, Walsh K (2011) Adipokines in inflammation and metabolic disease. *Nat Rev Immunol* 11: 85–97
- Pearce EL, Walsh MC, Cejas PJ, Harms GM, Shen H, Wang LS, Jones RG, Choi Y (2009) Enhancing CD8 T-cell memory by modulating fatty acid metabolism. *Nature* 460: 103–107
- Pei S, Huang M, Huang J, Zhu X, Wang H, Romano S, Deng X, Wang Y, Luo Y, Hao S *et al* (2021) BFAr coordinates TGFB signaling to modulate Th9-mediated cancer immunotherapy. *J Exp Med* 218: e20202144

- Portnoy VA, Scott DA, Lewis NE, Tarasova Y, Osterman AL, Palsson B (2010) Deletion of genes encoding cytochrome oxidases and quinol monooxygenase blocks the aerobic-anaerobic shift in *Escherichia coli* K-12 MG1655. *Appl Environ Microbiol* 76: 6529–6540
- Raud B, Roy DG, Divakaruni AS, Tarasenko TN, Franke R, Ma EH, Samborska B, Hsieh WY, Wong AH, Stuve P et al (2018) Etomoxir actions on regulatory and memory T cells are independent of Cpt1a-mediated fatty acid oxidation. *Cell Metab* 28: 504–515
- Reilly SM, Saltiel AR (2017) Adapting to obesity with adipose tissue inflammation. *Nat Rev Endocrinol* 13: 633–643
- Rigano D, Sirignano C, Tagliabatella-Scafati O (2017) The potential of natural products for targeting PPAR α . *Acta Pharm Sin B* 7: 427–438
- Rosen ED, Spiegelman BM (2014) What we talk about when we talk about fat. *Cell* 156: 20–44
- Schetz M, De Jong A, Deane AM, Druml W, Hemelaar P, Pelosi P, Pickkers P, Reintam-Blaser A, Roberts J, Sakr Y et al (2019) Obesity in the critically ill: a narrative review. *Intensive Care Med* 45: 757–769
- Sell H, Habich C, Eckel J (2012) Adaptive immunity in obesity and insulin resistance. *Nat Rev Endocrinol* 8: 709–716
- Shi LZ, Wang R, Huang G, Vogel P, Neale G, Green DR, Chi H (2011) HIF1 α -dependent glycolytic pathway orchestrates a metabolic checkpoint for the differentiation of TH17 and Treg cells. *J Exp Med* 208: 1367–1376
- Singh S, Dulai PS, Zarrinpar A, Ramamoorthy S, Sandborn WJ (2017) Obesity in IBD: epidemiology, pathogenesis, disease course and treatment outcomes. *Nat Rev Gastroenterol Hepatol* 14: 110–121
- Swinburn BA, Sacks G, Hall KD, McPherson K, Finegood DT, Moodie ML, Gortmaker SL (2011) The global obesity pandemic: shaped by global drivers and local environments. *Lancet* 378: 804–814
- Vaeth M, Maus M, Klein-Hessling S, Freinkman E, Yang J, Eckstein M, Cameron S, Turvey SE, Serfling E, Berberich-Siebelt F et al (2017) Store-operated Ca(2+) entry controls clonal expansion of T cells through metabolic reprogramming. *Immunity* 47: 664–679
- van der Windt GJ, Everts B, Chang CH, Curtis JD, Freitas TC, Amiel E, Pearce EJ, Pearce EL (2012) Mitochondrial respiratory capacity is a critical regulator of CD8+ T cell memory development. *Immunity* 36: 68–78
- Van Raemdonck K, Umar S, Szekanecz Z, Zomorodi RK, Shahrara S (2018) Impact of obesity on autoimmune arthritis and its cardiovascular complications. *Autoimmun Rev* 17: 821–835
- van Winden WA, Wittmann C, Heinze E, Heijnen JJ (2002) Correcting mass isotopomer distributions for naturally occurring isotopes. *Biotechnol Bioeng* 80: 477–479
- Versini M, Jeandel PY, Rosenthal E, Shoenfeld Y (2014) Obesity in autoimmune diseases: not a passive bystander. *Autoimmun Rev* 13: 981–1000
- Vishvanath L, Gupta RK (2019) Contribution of adipogenesis to healthy adipose tissue expansion in obesity. *J Clin Invest* 129: 4022–4031
- Wang R, Dillon CP, Shi LZ, Milasta S, Carter R, Finkelstein D, McCormick LL, Fitzgerald P, Chi H, Munger J et al (2011) The transcription factor Myc controls metabolic reprogramming upon T lymphocyte activation. *Immunity* 35: 871–882
- Wang N, Keszei M, Halibozek P, Yigit B, Engel P, Terhorst C (2016) Slamf6 negatively regulates autoimmunity. *Clin Immunol* 173: 19–26
- Xiong J (2018) Fatty acid oxidation in cell fate determination. *Trends Biochem Sci* 43: 854–857
- Yin Y, Choi SC, Xu Z, Perry DJ, Seay H, Croker BP, Sobel ES, Brusko TM, Morel L (2015) Normalization of CD4+ T cell metabolism reverses lupus. *Sci Transl Med* 7: 274ra218
- Yu T, Gan S, Zhu Q, Dai D, Li N, Wang H, Chen X, Hou D, Wang Y, Pan Q et al (2019) Modulation of M2 macrophage polarization by the crosstalk between Stat6 and Trim24. *Nat Commun* 10: 4353
- Zhang Y, Kurupati R, Liu L, Zhou XY, Zhang G, Hudaihed A, Filisio F, Giles-Davis W, Xu X, Karakousis GC et al (2017) Enhancing CD8(+) T cell fatty acid catabolism within a metabolically challenging tumor microenvironment increases the efficacy of melanoma immunotherapy. *Cancer Cell* 32: 377–391
- Zhang Y, Liu RB, Cao Q, Fan KQ, Huang LJ, Yu JS, Gao ZJ, Huang T, Zhong JY, Mao XT et al (2019) USP16-mediated deubiquitination of calcineurin controls peripheral T cell maintenance. *J Clin Invest* 129: 2856–2871
- Zhu C, Ji X, Zhang H, Zhou Q, Cao X, Tang M, Si Y, Yan H, Li L, Liang T et al (2018) Deubiquitylase USP9X suppresses tumorigenesis by stabilizing large tumor suppressor kinase 2 (LATS2) in the hippo pathway. *J Biol Chem* 293: 1178–1191
- Zhu Q, Yu T, Gan S, Wang Y, Pei Y, Zhao Q, Pei S, Hao S, Yuan J, Xu J et al (2020) TRIM24 facilitates antiviral immunity through mediating K63-linked TRAF3 ubiquitination. *J Exp Med* 217: e20192083